RIGA TECHNICAL UNIVERSITY

Nikolajs Toropovs

EVALUATION OF HIGH-PERFORMANCE CONCRETE EXPOSED TO ELEVATED TEMPERATURES

Summary of the Doctoral Thesis

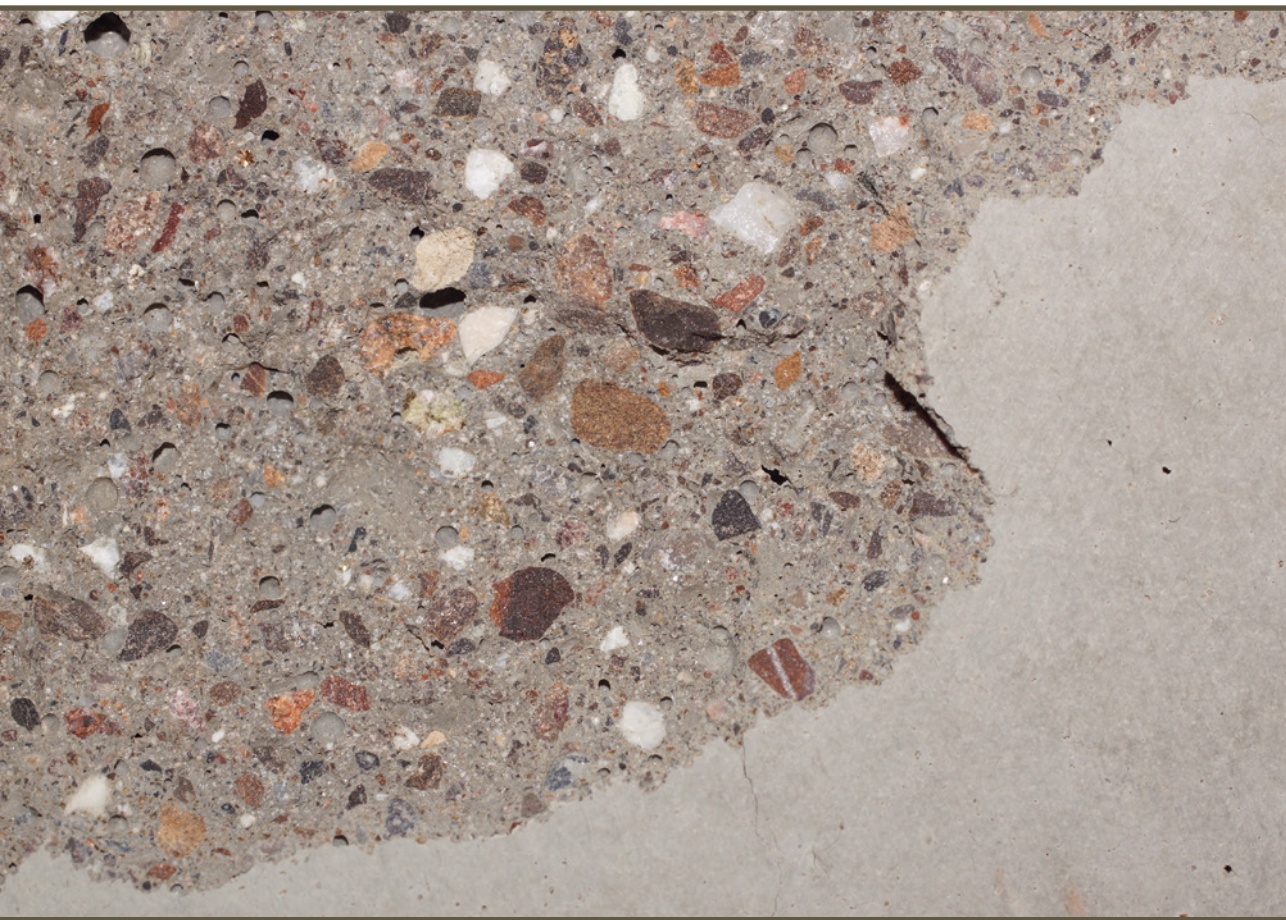

RTU Press
Riga 2026

RIGA TECHNICAL UNIVERSITY
Faculty of Civil and Mechanical Engineering
Institute of Sustainable Building Materials and Engineering Systems

Nikolajs Toropovs
Doctoral Student of the Study Programme "Civil Engineering"

EVALUATION OF HIGH-PERFORMANCE CONCRETE EXPOSED TO ELEVATED TEMPERATURES

Summary of the Doctoral Thesis

Scientific supervisor
Associate Professor Dr. sc. ing.
GENĀDIJS ŠAHMENKO

RTU Press
Riga 2026

Toropovs, N. Evaluation of High-Performance Concrete Exposed to Elevated Temperatures. Summary of the Doctoral Thesis. – Riga: RTU Press, 2026. – 55 p.

Published in accordance with the decision of the Promotion Council "RTU P-06" from 10th of October 2025, No. 04030-9.6/16.

This study was partially funded by the Scientific Exchange Program Sciex NMS-CH under the project 12.305 "FRESCO-Fire spalling of High Performance and Ultra-High Performance Concrete".

Acknowledgements

Slow long walks give you more time to observe and enjoy nature. To be fancy, I would like to quote FN here: "All truly great thoughts are conceived while walking". And I took my time.

I would like to express my sincere gratitude to my supervisors, who inspired me and led by example with true dedication and enthusiasm: Genādijs Šahmenko, Pietro Lura, Mateusz Wyrzykowski, Michele Griffa and Benedikt Weber.

I am also grateful to reviewers and members of my Promotion Council for their constructive feedback and thoughtful suggestions.

I would like to thank my colleagues and collaborators for being involved in great projects beyond what I could imagine at the start of my Lab expedition as a bachelor student.

This has been a remarkable journey through the decades, shaped by the many people I have met along the way. Thank you, Alex, Aleksandrs, Alessio, Alina, Andrejs, Andreas, Barbara, Dani, Daniele, Davide, Diana, Ellina, Emilie, Fei, Frank, Gabi, Grazia, Guntis, Iuri, Jānis, Köbi, Lauris, Latina, Malene, Marcel, Martin, Mārtiņš, Nadine, Paulina, Petra, Raphael, Robert, Roman, Rupert, Sarah, Sebi, Sepp, Serena, Vincent, Vitālijs, Walter, Zhangli.

I have had enough time to observe and reflect – an experience that has been a true blessing.

Finally, I would like to thank my family for their constant support.

Cover picture by Nikolajs Toropovs.

https://doi.org/10.7250/9789934372643

ISBN 978-9934-37-264-3 (pdf)

DOCTORAL THESIS PROPOSED TO RIGA TECHNICAL UNIVERSITY FOR PROMOTION TO THE SCIENTIFIC DEGREE OF DOCTOR OF SCIENCE

To be granted the scientific degree of Doctor of Science (PhD), the present Doctoral Thesis has been submitted for defence at the open meeting of RTU Promotion Council on 26 February 2026 at 11.00, at the Faculty of Civil and Mechanical Engineering of Riga Technical University, Ķīpsalas iela 6B/6A, Room 546.

OFFICIAL REVIEWERS

Dr. sc. ing. Andrejs Pupurs
Riga Technical University

Dr. phys. Andris Jakovičs
University of Latvia, Latvia

Professor Dr. Valentin Antanovič
Vilnius Gediminas Technical University, Lithuania

DECLARATION OF ACADEMIC INTEGRITY

I hereby declare that the Doctoral Thesis submitted for review to Riga Technical University for promotion to the scientific degree of Doctor of Science (PhD) is my own. I confirm that this Doctoral Thesis has not been submitted to any other university
for promotion to a scientific degree.

Nikolajs Toropovs ……. (signature)
Date: ……

The Doctoral Thesis has been written in English. It consists of an Introduction, four chapters, Conclusions, 84 figures, 14 tables, and two appendices; the total number of pages is 126, including appendices. The Bibliography contains 148 titles.

CONTENTS

INTRODUCTION

Through the long history of research, development and application, concrete has become the most used manmade material in the world[1–3]. It has found applications both as a simple road barrier block to organize the traffic and as a structural material to reach heights and spans hard to imagine decades ago. Call for concrete with superior strength and durability properties compared to traditional concrete came alongside industrial development in the second half of the 20th century. Concrete has undergone changes to ensure better performance overall and greater specialization to meet requirements in the field of application. This involved optimization of grain size distribution, use of fine particles with pozzolanic activity, use of aggregates with certain properties, etc[4]. However, most important was the decrease of water to cement ratio and introduction of water reducing admixtures. Water reducing admixtures were introduced in the 1930s and affected the concrete industry; however, it was in the 1980s, when the new type of polycarboxylate plasticizers led to a revolution in concrete properties[5]. Concrete with superior properties compared to ordinary concrete (OC) is often called high performance concrete (HPC), and the plasticizers that revolutionized the market are referred to as superplasticizers. HPC is characterized by high compressive and tensile strengths, high modulus of elasticity, good durability, low permeability and high resistance to abrasion. By reducing the construction dead weight, fewer raw materials are consumed and slender, elegant constructions with lower embodied energy become possible. Changes in concrete compositions and performance happened gradually, and there is no clear single borderline between OC and HPC; a variety of applications and availability of raw materials allows co-existence of unlimited mix designs worldwide. Special and at the same time very diverse applications, such as tunnels, high-rise buildings, nuclear power plants, long-span bridges, led to high diversity in types of concrete and new challenges that were not in the spotlight years ago. All this allows the coexistence of “new” mix designs without running “old” concepts completely out of date. Discussing the significant development in the concrete industry over the 20th century, Neville and Aitcin compared it to the telecommunication and car industry – “the changes are nowhere near as revolutionary as the changes in telecommunication and even in motor cars”[6].

It is necessary to ensure long durability of structures, both from a labor efficiency point of view and from sustainable development of society in a world of limited mineral/fossil resources. Manufacturing of cement is responsible for up to 8–9 % share of global man-produced CO_2[3], reaching 163 million tons of cement products in EU28 countries alone in 2016, with its maximum at 268 million tons in 2007[7]. In 2015, 167 million tons of cement were produced in EU28 countries, representing 4 % of global production, making the EU the third largest producer of cement worldwide, after India with its 270 million tons and China dominating the market with 2350 million tons of cement, which corresponds to 51 % of global production in 2015[7]. Calcination of limestone and fuel combustion to produce cement, combined, release approximately 1 ton of CO_2 per 1 ton of cement.[3]

Despite the rapid development of concrete properties and a large volume of material produced, emphasizing the importance of concrete to modern society, one of the major limitations to the worldwide spread of HPC comes from its performance under fire, namely, a poor resistance of HPC when exposed to high temperatures. This is because of the violent damage mode referred to as explosive spalling[4, 8]. Explosive spalling at high temperature can lead to a gradual loss of the protective concrete layer of reinforcement, exposing it to the

environment, and ultimately to the failure of a reinforced structural concrete member. It is important to distinguish spalling as a complex, structure related phenomena, and the changes that concrete undergoes at different temperatures as a material. The difference is discussed in Sections 1.1 and 1.2 of this Thesis, from the point of view of the structure and as for material correspondingly.

The more HPC comes into application, the higher the concern about HPC performance in the event of fire. With increased use of HPC in high-rise buildings and tunnels, it becomes necessary to study the nature of explosive spalling under fire to address those concerns and to find a reliable solution to protect new and existing structures from spalling. The high interest of research and industry communities in spalling was triggered in part by large-scale fire disasters that shook the public. In the 90s of the last century, a number of large fires happened in tunnels (in the Great Belt tunnel in 1994, in Channel Tunnel [9] in 1996, and in the Mont Blanc tunnel in 1999), causing serious and expensive damage; those three fires were summarized and discussed by Khoury[10].

On November 18, 1996, a fire occurred in the railroad tunnel connecting France and England, known as the Channel Tunnel. A locomotive with 10 train wagons and 9 trucks burned for about 10 hours, resulting in severe structural damage and 8 people injured. The costs due to damage to vehicles and the tunnel, alongside costs related to the disruption of services, were as high as £50 million, according to Kodur[11]. Maximal temperatures reached varied from 700 °C [9, 12] to 1000 °C [11]. Ulm [9, 12] reported economic losses alone reaching around $1.5 million per day over 6 months of repairs when the tunnel was closed. The Tunnel was formed of 45 cm thick precast reinforced concrete rings; hundreds of meters of tunnel were damaged as a result of fire, with an average depth of spalling from 10 cm to 20 cm. In some parts of the tunnel, concrete rings were destroyed up to the chalk substratum[11]. This indicates the significance of damage caused by fire and the need for a deeper understanding of mechanisms of spalling.

There are a number of methods that have been proven capable of preventing or decreasing explosive spalling, e.g. addition of fibers. However, due to a lack of clear guidelines and a single fire scenario, there is no general protective method validated by a fire test. To facilitate wide and safe application of HPC, fire safety design and protective methods have to be based on a deep understanding of processes underlying explosive spalling and evolution of material properties in case of fire.

The new imaging and characterization methods developed in recent years, applied together on a unified set of materials, enable us to deliver new insight into the fundamental mechanisms of fire spalling, with the overall goal of eventually improving the fire resistance of HPC.

GOALS OF THE THESIS

The goal of the Thesis is to validate complex non-destructive measuring techniques from other fields to evaluate thermal damage of concrete.

OBJECT OF THE THESIS

This study gives the qualitative and quantitative evaluation of super absorbent polymers (SAP) as an admixture to limit damage induced by elevated temperatures. The nonlinearity of the samples accessed by means of nonlinear resonance ultrasound spectroscopy highlights the

combined effect of SAP and PP fibers on the state of the material, both before and after the thermal loads.

The new imaging and characterization methods developed in recent years put all together on a unified set of materials enables the author to deliver new insight into the fundamental mechanisms of fire spalling, with the overall goal of eventually improving the fire safety of HPC.

OBJECTIVES OF THIS THESIS

To reach the goals, the following objectives are set:

- summarize effect of elevated temperatures on concrete from the literature, with focus on residual properties of concrete;
- identify the fundamental parameters that facilitate or prevent spalling by studying an ordinary concrete (OC) mix that would never experience explosive thermal spalling and a plain high-performance concrete (HPC) matrix that would experience spalling under the same conditions;
- modify the HPC matrix with admixtures to limit or eliminate spalling;
- investigate residual structure and residual mechanical properties of all the mixes over time and due to thermal treatment at elevated temperatures;
- investigate thermal damage of concrete by means of non-destructive methods; establish methods for quantitative evaluation of the damage.

SCIENTIFIC NOVELTY OF THE STUDY

This Thesis provides a systematic study of a broad set of concrete properties under well-controlled, unified conditions.

To the best of the author's knowledge, for the first time, an actual spalling was recorded during neutron radiography measurements. Owing to a high attenuation of the neutron beam by hydrogen, neutron imaging allows the study of the distribution of water in cement-based materials. The neutron radiography was carried out on samples of mortar while exposed to high temperatures. To this end, the samples were placed on a heating plate with specially designed protective shields to protect the delicate neutron imaging setup (in particular scintillator) from explosive debris. This allowed for a unique result – online observation of the moisture distribution in the sample as the spalling began.

To the author's knowledge, for the first time, complex real-time measurements of vapor pressure in the pores, temperature gradients in the material, neutron radiography and the thermal loading of the sample were simultaneously combined.

For the very first-time effect of SAP on thermal damage of concrete was evaluated by non-destructive methods.

For the very first time, three ultrasonic methods were used to evaluate thermal damage of concrete, and the obtained ultrasonic data is supported by micro computed tomography (uCT) of the very same specimens before and after thermal damage.

APPROBATION OF RESULTS AND PUBLICATIONS

The main journal articles

1. Toropovs, N., Monte, F. L., Wyrzykowski, M., Weber, B., Sahmenko, G., Vontobel, P., Felicetti, R. & Lura, P. (2015). Real-time measurements of temperature, pressure and moisture profiles in High-Performance Concrete exposed to high temperatures during neutron radiography imaging. *Cement and Concrete Research*, *68*, 166–173.
2. Zhu, P., Brunner, S., Zhao, S., Griffa, M., Leemann, A., Toropovs, N., Malekos, A., Koebel, M. & Lura, P. (2019). Study of physical properties and microstructure of aerogel-cement mortars for improving the fire safety of high-performance concrete linings in tunnels. *Cement and Concrete Composites*, *104*, 103414.
3. Dauti, D., Tengattini, A., Dal Pont, S., Toropovs, N., Briffaut, M., & Weber, B. (2018). Analysis of moisture migration in concrete at high temperature through in-situ neutron tomography. *Cement and Concrete Research*, *111*, 41–55.
4. Dauti, D., Tengattini, A., Pont, S. D., Toropovs, N., Briffaut, M., & Weber, B. (2020). Some observations on testing conditions of high-temperature experiments on concrete: An insight from neutron tomography. *Transport in Porous Media*, *132*(2), 299–310.
5. Dauti, D., Dal Pont, S., Weber, B., Briffaut, M., Toropovs, N., Wyrzykowski, M., & Sciumé, G. (2018). Modeling concrete exposed to high temperature: Impact of dehydration and retention curves on moisture migration. *International Journal for Numerical and Analytical Methods in Geomechanics*, *42*(13), 1516–1530.

1. CONCRETE SUBJECTED TO HIGH TEMPERATURES. THE SUMMARY OF THE LITERATURE STUDY

1.1. EFFECT OF HIGH TEMPERATURES ON STRUCTURES

The performance of the structure under fire depends on many factors. Attempts to summarize these factors and develop regulations to test structures exposed to fire date back to 1903, when the first testing standard of fire resistance was introduced[13] during the Fire Prevention Congress in London in 1903.

Failure of structures could occur due to deterioration of the mechanical properties of concrete or the reinforcing steel, loss of bond with reinforcing steel, or spalling of concrete. Structural element has to be designed to fulfil its load-bearing functions for a required time in a given fire scenario. According to EN 1992-1-2[14], both the nominal fire scenario and the parametric fire approach can be used to ensure the safety of the structure. Structural Eurocodes deal with passive fire protection of structures in terms of designing structures and members.

As the most straightforward and obvious effect of fire on any material or structure is the direct exposure to flame, it is generally known that concrete and its steel reinforcement do not burn. They do not emit toxic fumes, do not produce dangerous smoke and do not lose molten particles. Yet, during a fire, the structures are at risk of failure because the mechanical properties (strength) of concrete and, even more so, of steel, reduce significantly. The spalling is dangerous because i) it exposes the steel reinforcement to high temperatures and hence leads to its faster thermal deterioration; ii) it leads to the loss of bond with the reinforcement locally; and iii) in extreme cases leads to a decrease in the cross-sectional area of the concrete members.

Two main types of fire load curves are the cellulosic fire curve and the hydrocarbon (HC) fire curve. The main difference is the time it takes to reach its maximum temperature, where burning rate in cellulosic fires is comparably slower due to “fuel” for fire are building materials and content of building, while temperature rise in hydrocarbon fires is significantly faster as “fuel” for fire are hydrocarbons in petrochemical facilities or actual fuel in the cars, as for fire in tunnels and parking facilities. Fewer tests are performed applying the jet fuel fire scenario curve, where the maximal temperature rise is instant.

A complex large-scale fire test was carried out in 2003 in Norway; the unused Runehamar tunnel became a testing facility, where five large-scale fire tests were carried out. A large amount of data was obtained[15–18], and described in detail, e.g. gas temperature[16], fire spread and flame length[17] and heat release rates[18]. Tests made a significant impact and highlighted the extreme conditions of fire in tunnels. During test T1[15], maximal temperature of 1359.6 °C was recorded; it is to note, that the fire load was generated by HGV trailer mock-up made of 360 wood pallets (1200 × 800 × 150 mm^3 in size), 20 wood pallets (1200 × 1000 × 150 mm^3 in size), 74 PE plastic pallets (1200 × 800 × 150 mm^3 in size) and 122 m^2 polyester tarpaulin. This temperature significantly exceeded the temperatures of the cellulosic fire curve that was expected from wooden pallets and was still higher than the HC curve. The International Tunnelling Association took into account the data obtained in the Runehamar tunnel fire test in their guidelines[19] and recommended to follow RWS curve scenario for road tunnels. While an

actual fire test in the tunnel is a very special case, smaller-scale tests of tunnel elements have practical meaning and result in valuable data to predict the actual behavior of the tunnel lining in the case of fire.

Based on previous experience and extreme fire cases that led to multiscale damage, more and more sophisticated and extreme fire tests are performed to increase the safety of important structures. Large-scale testing objects are built to achieve realistic fire conditions in order to improve the safety of the actual structure. A great example is the Hong Kong-Zhuhai-Macao immersed tunnel built in scale 1/5, where external load and fire from two sides were ensured[20]. As a result of this large-scale test, Dong *et al.*[20] observed almost 100 % spalling of the interior area of the tunnel, with a maximum depth up to 142.2 mm.

This being said, the effect of concrete structures being exposed to severe fire leads not only to serious damage and high expenses but also stresses the necessity to study the nature of damage and implement changes in building codes.

1.2. EFFECT OF HIGH TEMPERATURES ON MATERIALS

The spalling is a structurally related damage mechanism in the sense that it depends upon geometrical, external load and kinetic factors, occurring in addition to the material changes, being a static function of temperature only. In this section, only the latter aspect, which is the residual effect of temperature on material properties, is considered. It should be stressed that it is not always possible to fully decouple the other factors (e.g. geometry or kinetics) from the net effect of temperature. This is usually done by studying possibly slow temperature changes and small sample sizes.

Here, it is important to distinguish the temperature of the fire from the actual temperature at any point of the material. While fire curves determine the temperature of fire/gases, a gradient of temperatures is expected in a real structure, changing in time.

Obtaining the most exact and wide, complementary properties of concrete as it overcomes changes caused by fire load at each time/temperature step is not an easy challenge. Spalling phenomena discussed in this Thesis are related to the performance of the structure at high temperatures, which means that the material itself experiences mechanical and thermal loads at the same time. From a testing point of view, this means that samples used to measure mechanical, transport or other properties have to be simultaneously mechanically and thermally loaded, which is not a safe working/testing environment in most of the cases.

The most common assessment of the effect of high temperatures on material is done by presenting the data of mechanical properties over a range of temperatures and describing changes in microstructure due to thermal loads. Some of the properties described in the literature are summarized below. It is important to notice that most of the mechanical properties summarized below are obtained after cooling down the samples, i.e. in the residual state.

Compressive strength

Data summarized below is adapted from a number of studies[21–42] and is presented as a ratio of residual properties to the same property before thermal treatment; data is recalculated from the tables as well from the figures, and might have a slight deflection from the raw data of those studies (see Fig. 1.1). For example, the evolution of residual compressive strength over

temperatures is presented for 101 mixes of concrete. In most of the papers temperature of the thermally non-treated samples is defined as 20 °C, 25 °C or 30 °C, where the initial temperature is not defined numerically and is stated as "room temperature". For the matter of plotting the data, "room temperature" is assumed to be 20 °C, for example, data from the paper by Irshidat[29].

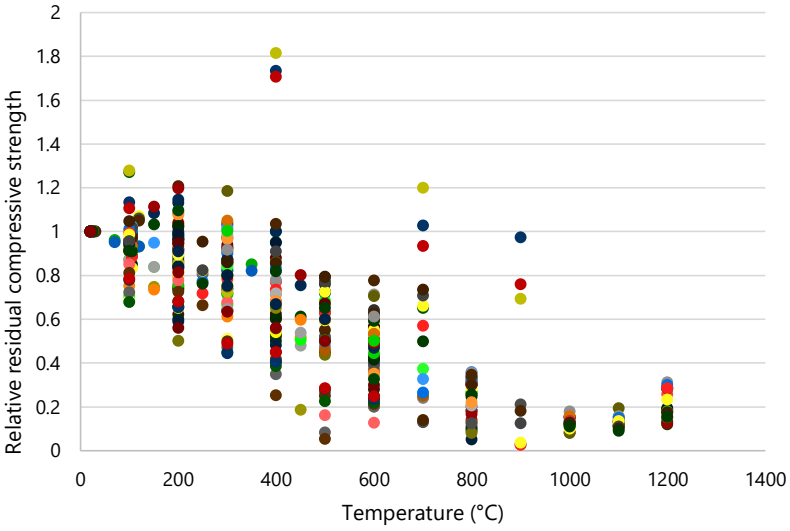

Fig. 1.1. Relative residual compressive strength, data adapted from[21–42].

Modulus of elasticity

Fig. 1.2 summarizes research data on residual Young's modulus adapted from studies[25, 27, 29, 33, 36, 39, 41, 42] conducted on different types of concrete, to represent a general trend of evolution of elasticity after treatment at high temperatures.

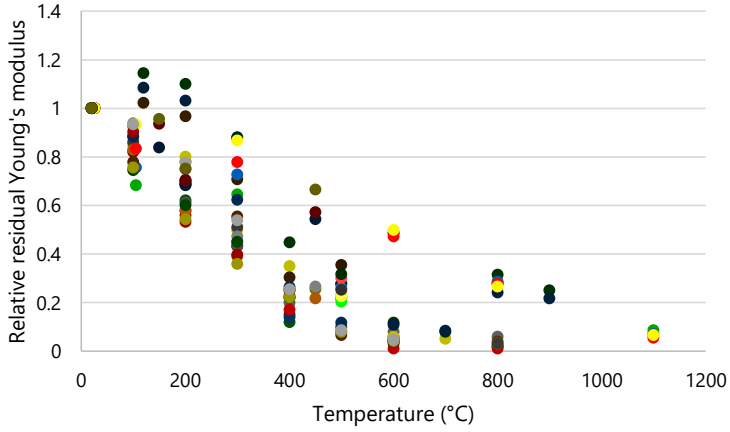

Fig. 1.2. Relative residual Young's modulus.

Slightly higher relative residual Young's modulus is observed for reactive powder concretes studied by Zheng[39], who reports an increase of Young's modulus at temperature 200 °C and below (see Fig. 1.2).

Lau and Anson[42] studied the effect of steel fibers on the properties of concrete after exposure to high temperatures. Mixes with steel fibers showed higher modulus of elasticity than reference mixes with no fibers at all temperatures (study was conducted within a 25–1100 °C range).

Porosity

Summary of residual changes of porosity at high temperatures is presented in Fig. 1.3. Mercury intrusion porosimetry (MIP) was used in the studies[35, 37, 40, 42, 43], similarly to this Thesis.

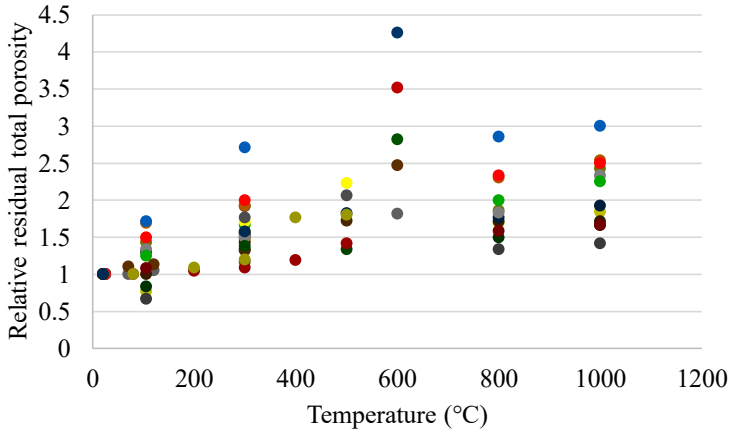

Fig. 1.3. Relative residual total porosity.

Changes in hydration products

Exposure of concrete to high temperatures results not only in physical damage but also causes moisture movement and dehydration of hydrates. A collection of thermal analysis data on the decomposition of phases at temperatures 0 °C to 800 °C is provided by Collier[44]. While decomposition of pure phases can be measured with methods of Thermogravimetric Analysis (TGA), in real life structure, the processes are more complex, as structural element has temperature gradients in case of fire and pressure build up is very likely, affecting temperature of decomposition of hydrates. At the same time, as the nature of phase change, like dehydration or decarbonation, is an endothermic reaction, this means a decrease in temperature if no new energy input is provided.

General reactions of dehydration are provided in the cement chemist's nomenclature:

$$C_8AFS_2H_{22} \xrightarrow{T_{onset}=40\ °C} C_4AF + 2CH + 2CS + 22H; \quad (1.1)$$

$$C_3S_2H_3 \xrightarrow{T_{onset}=110\ °C} C_3S_2 + 3H; \quad (1.2)$$

$$CH \xrightarrow{T_{onset}=430\ °C} C + H. \quad (1.3)$$

As seen from **Error! Reference source not found.**) and **Error! Reference source not found.**), the products of decomposition can further decompose at higher temperatures.

While straightforward composition and decomposition of pure phases is a well-studied topic, the dynamic phase composition during decomposition of other phases in conditions of elevated temperatures is rather complicated. A complex model predicting dynamic phase composition at temperatures up to 1200 °C is proposed by Jiang *et al.*[45] The authors stress the importance of heating rates on the instantaneous formation of phases.

Integrity of material evaluated with non-destructive methods: Ultrasound-based measurements

The most common ultrasonic method to evaluate the state of concrete material is to measure ultrasound pulse velocity (UPV). It is discussed further in Section 4.2. The overall effect of high temperatures on the integrity of the material is presented here as relative residual ultrasound pulse velocity. Ultrasound pulse velocity is a linear single pulse method; it gives us information on the overall state of the material, as it is sensitive to macro cracks and less sensitive to micro damage.

Fig. 1.4 represents relative UPV measured on the samples at residual state, after being exposed to high temperature, where initial UPV (value = 1) was measured on the samples before exposure to high temperatures. Data were summarized from papers[23, 25, 27, 32].

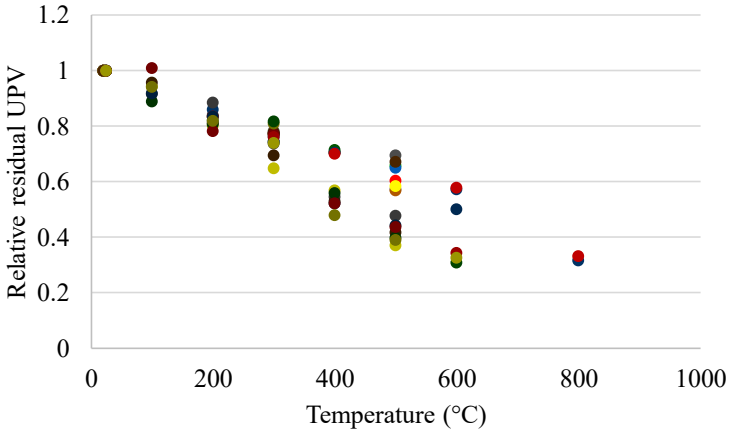

Fig. 1.4. Relative residual UPV.

1.3. FACTORS AND MECHANISMS OF EXPLOSIVE SPALLING IN CONCRETE STRUCTURES

The first theories on spalling mechanisms date back to the 1960's[46, 47]. See also the historical overview prepared by Jansson[13], where spalling of concrete under fire as an independent phenomenon raising interest in research society dates back to 1854[13]. According to the pressure build-up theory[46], water accumulates behind the drying front because vapor produced at the drying front migrates towards the colder inner region, where it condenses. The vapor pressure build-up concept is visualized by Ozawa and adapted here in Fig. 1.5.

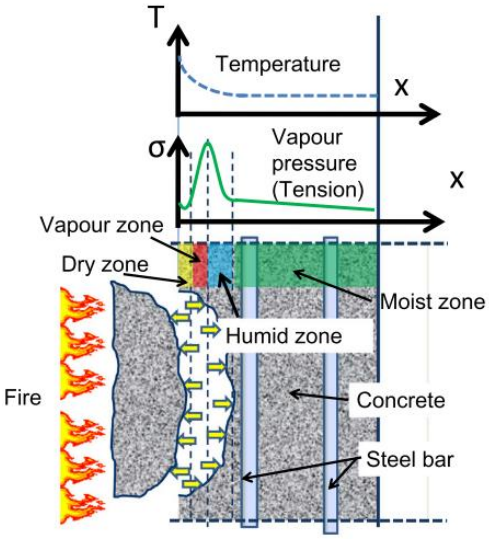

Fig. 1.5. Vapor pressure build-up concept, adapted from Ozawa.[48]

Another possible mechanism of spalling is described by the *thermal stresses theory*[47]. Since the temperature at the moisture clog is close to 100 °C and the surface temperature increases rapidly while the depth of the dry layer is still small, a steep thermal gradient develops between the heated surface and the moisture clog, which induces high thermal stresses. According to Saito[47], spalling is due to compression failure near the heated surface. Based on a detailed analysis of pore pressure and thermal stresses, Sertmehmetoglu[49] proposed that the compressive stresses near the heated surface result in tensile cracks parallel to the surface. The pressure developing in these cracks induces explosive spalling. Failure is further eased by stress concentration at the crack tips and by buckling due to compression. Sertmehmetoglu, in his Thesis[49], reproduces spalling of concrete at room temperature by creating overpressure in artificially created cracks that are parallel to the surface of the specimen.

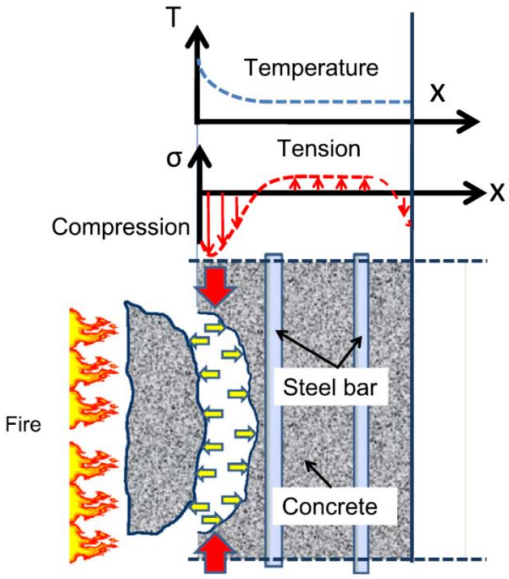

Fig. 1.6. Thermal tension concept, adapted from Ozawa.[48]

It needs to be underlined that the mechanisms proposed by the two theories (pressure build-up and thermal stress) are strongly coupled and both dependent upon the moisture distribution (and upon the formation of the moisture clog) during fire. Both processes progress at the same time and may influence the boundary conditions of each other, affecting the transport and mechanical properties of the material. Bažant sees the pore pressure as a "trigger of the explosive thermal spalling of high-strength concrete", while the state of material that leads to the failure is driven by "the amount of the energy stored due to thermal stresses"[50]. The idea of a trigger and a corresponding threshold value for spalling to occur is discussed by Lo Monte[51], who describes it as a link between decay of apparent tensile strength and pore pressure.

Along with the moisture clog theory, the BLEVE (boiling liquid expanding vapor explosion) phenomenon that occurs at slow heating rates should be mentioned. When no sharp temperature gradient is formed, the conditions in the two nearby regions/pores are very similar. Hence, because of the similar pressures and temperatures in the neighboring pores, there is no driving force for the mass or energy exchange between them. This is valid for the ideal case, two identical-shaped, same-size pores. As before, heating a pore contains air, water and water vapor. At higher temperatures, water evaporates; however, as conditions in the pore nearby are the same, vapor stays in the same pore, increasing the pressure. At increased pressure, the boiling point of water increases, leading to condensation and the presence of water in the liquid state within the pore. Liquid water occupies less space than vapor; however, when cracks appear, the sudden release of pressure takes place, resulting in instantaneous evaporation of superheated water, as the boiling point drops down to 100 °C. This can lead to explosive spalling because of sharp volume change and high-energy release due to the phase change[52].

The factors affecting the appearance and severity of spalling are:

- *maximal temperature*;
- *heating rate*;
- *heating profile;*

- *duration of fire*;
- *section size*;
- *shape of the heated elements*;
- *moisture content*;
- *pore pressure*;
- *permeability*;
- *age of concrete*;
- *strength of concrete*;
- *compressive stress and restraint*;
- *type of aggregates*;
- *type of fine fillers*;
- *aggregate size*;
- *cracks*;
- *reinforcement*;
- *cover of reinforcement;*
- *supplementary metal elements*;
- *steel fibers*;
- *polypropylene fibers*;
- *natural fibers*;
- *air-entrainment agents*.

The long list of factors affecting the performance of concrete structures under fire indicates the complexity of the spalling phenomenon and challenges in accurate qualitative prediction of its appearance, and, more importantly, quantitative estimation of the damage. Several factors are very closely linked and have a direct impact on each other; however, they do not mean the same.

1.4. PREVENTION OF EXPLOSIVE SPALLING IN CONCRETE STRUCTURES

To ensure safety, alongside fire detection, fire extinguishing systems, and the design of safe evacuation routes, several methods can be applied to the concrete structure itself to decrease or prevent fire spalling. Some methods can be implemented at the stage of mix design of the concrete or design of geometry and reinforcement of concrete elements; however, this is not applicable to already existing structures. Meanwhile, other methods are the only choice left for existing structures where additional protection is required.

1.5. SUMMARY

Review of the topic presented above highlights the complexity of the problem, both from the point of view of the material and of the structural elements, multiplied by the fire conditions.

The actual fire tests of large-scale structures are very challenging for interpretation, besides obvious spalling/no-spalling visual observation, and very expensive. However, the possible damage caused to the structure justifies the research efforts.

The data summarized from the literature indicate:

- deterioration of mechanical properties at high temperatures;
- risk to the integrity of the structure due to explosive spalling;
- complexity of physical and chemical changes that concrete undergoes in extreme temperature conditions;
- challenges in accessing the actual real-time state of material due to complexity and safety challenges during the hot tests;
- a combination of boundary conditions and the actual fire scenario can be very unpredictable;
- explosive spalling of concrete due to fire is not a property of material, but rather a complex combination of factors strongly linked with each other;
- various protection methods to limit or exclude the occurrence of explosive fire spalling, where layers of fire protection material are a common solution for existing structures, and the addition of natural and PP fibers has proven its performance for new structures.

2. MATERIALS AND MIX COMPOSITIONS AS OBJECTS OF THIS STUDY

2.1. MATERIALS

The study described focuses on the evaluation of the effect of high temperatures on the microstructure of concrete with Portland cement as a binder, and the applicability of different methods to investigate changes that concrete undergoes due to thermal loading.

To decrease uncertainty stemming from the complex composition of the blended binders, the author chose ordinary Portland cement Jura CEM I 52.5 R. The oxide composition of cement is presented in Table 2.1.

Table 2.1

Oxide Composition of Jura CEM I 52.5 R

Oxide composition	Mass (%)
SiO_2	19.64
Al_2O_3	5.26
Fe_2O_3	3.13
Cr_2O_3	0.009
MnO	0.057
TiO_2	0.290
P_2O_5	0.179
CaO	63.18
MgO	2.00
K_2O	1.01
Na_2O	0.16
SO_3	2.94
LOI*	1.87
total	99.72

*LOI – loss on ignition

Deionized water was used for mixing to exclude traces of materials not related to this study. Locally widely available alluvial sand and gravel were used as aggregates.

To obtain a denser and well-packed structure, silica fume Elkem U968 was used. To reduce the w/c ratio and maintain good workability, polycarboxylate-based superplasticizer Sika-56 was used. Polypropylene fibers Fibermesh 150-3 from Propex with specific gravity 0.91 and fiber length of 3 mm were used. The melting point of Fibermesh 150-3 is 162 °C, temperature of ignition is 593 °C. SAP VP300 from BASF was used to ensure internal curing[53] of HPC samples.

2.2. MIX COMPOSITIONS

As described above, the phenomenon of explosive spalling occurs in dense and less permeable concrete, like high-performance and ultra-high performance concrete (HPC and

UHPC). To evaluate which combination of properties leads to spalling and which does not, we need both: a mix that would spall virtually always and a mix that would virtually never spall under the same conditions. Both should have practical application and reasonable strength properties to have potentially wide use in load-bearing structures.

All the mixes are presented in Table 2.2.

Table 2.2

Mix Compositions Investigated in this Study

Mortar type	OC	HPC-ref	HPC+PP	HPC+SAP	HPC+PP+SAP	HPC_16 mm
Cement CEM I 52.5 R	370	488	488	464	464	488
Silica fume	0	122	122	116	116	122
Aggregates 0–1 mm	740	633	633	633	633	253
Aggregate 1–4 mm	1110	949	949	949	949	380
Aggregates 4–8 mm	0	0	0	0	0	396
Aggregates 8–16 mm	0	0	0	0	0	554
Superplasticizer	5.18	8.54	8.54	8.12	14.5	8.54
PP fibers	0	0	2	0	2	0
SAP	0	0	0	1.93	1.93	0
Water	185	189.1	189.1	197.2	197.2	189.1
w/b total	0.5	0.31	0.31	0.34	0.34	0.31

As you can see from the table above, the amount of aggregates was kept the same for all HPC mixes; however, the mass of cement per m^3 was changing.

2.3. EVALUATION OF MIXES BY SPALLING/NO-SPALLING CRITERIA

To study explosive spalling of concrete and investigate the evolution of properties over age and temperatures, one has to ensure that the mix compositions presented in Table 2.2 would include both spalling and no-spalling performance. Where OC mix should not spall, HPC-ref mix would spall. Next, by adding spalling preventive additives to the original HPC-ref mix, new mixes would be obtained that experience less severe or no spalling (HPC+PP, HPC+SAP and HPC+PP+SAP).

Results of fire-spalling performance

Results are summarized as spalling/no-spalling in Table 2.3, where C denotes cubes and P denotes plates. The number next to sample indications corresponds to the number of samples where spalling was observed (out of the total number of samples tested), e.g. 0/2 means that no samples spalled out of 2 samples tested; 2/2 means that spalling was observed on 2 out of 2 samples.

Table 2.3

Summary of Spalling Tests

Age	OC	HPC-ref	HPC+PP	HPC+SAP	HPC+PP+SAP	HPC_16mm
1d	C 0/2; P 0/1	C 2/2; P 1/1	C 0/2; P 0/1	C 2/2; P 1/1	C 2/2; P 0/1	C 2/2
3d	C 0/2; P 0/1	C 2/2; P 1/1	C 0/2; P 0/1	C 2/2; P 1/1	C 0[1]/2; P 0/1	C 2/2
7d	C 0/2; P 0/1	C 2/2; P 1/1	C 0/2; P 0/1	C 2/2; P 1/1	C 1/2; P 0/1	C 2/2
21d	C 0/2; P 0/1	C 2/2; P 1/1	C 0/2; P 0/1	C 2/2; P 1/1	C 0/2; P 0/1	C 2/2
28d	C 0/2; P 0/1	C 2/2; P 1/1	C 0/2; P 0/1	C 2/2; P 1/1	C 0/2; P 0/1	C 2/2
35d	C 0/2; P 0/1	C 2/2; P 1/1	C 0/2; P 0/1	C 2/2; P 1/1	C 0/2; P 0/1	C 2/2

Alongside a general evaluation of spalling/no-spalling criteria, the time of spalling was recorded.

[1] One of the cube specimens spalled 30 minutes after the end of the thermal loading, out of the assumed test time.

3. EFFECT OF ELEVATED TEMPERATURES ON PROPERTIES AND MICROSTRUCTURE OF CONCRETE

3.1. INTRODUCTION

In the previous chapter, the results of concrete exposed to high temperatures from one side are summarized as simple spalling/non-spalling criteria. Here, the complexity of the processes resulting in either spalling or non-spalling is tracked through the changes in properties and microstructure of the material after exposure to elevated temperatures. As mentioned in Section 1.2, due to safety reasons and to acquire a wide range of data on a unified set of materials, the residual state is investigated. This enables the delivery of new insight into the fundamental mechanisms of fire spalling. The data provided below was partially used to improve a numerical model describing the behavior of concrete exposed to high temperatures.[54]

The rate of temperature increase was approximately 16 °C/min. The reason for the fixed heating rate in the oven is to bring it to the same heating rate as the heating plate used for spalling/no-spalling evaluation and neutron radiography study, described in Section 4.1. This way, all the data is more uniform and compatible.

3.2. METHODS

Mechanical properties

The mechanical properties of the mortars were determined on 40 × 40 × 160 mm^3 prismatic specimens. Thermal loading was performed at the age of 28 days, by bringing the specimens to temperatures of 120 °C, 200 °C, 400 °C and 600 °C, followed by 8 h at the maximum temperature and then free cooling down in the furnace.

Young's modulus, flexural strength and compressive strength were determined at the ages of 1, 3, 7, 21, 28 and 35 days on samples stored in parallel at room temperature (further referred to as the virgin state).

Hydration and dehydration of concrete (TGA)

To study initial bound water content and dehydration at high temperatures, thermogravimetric analysis (TGA) tests were performed. Samples of all mortar mixes (Table 2.2) were tested at 1, 3, 7, 21, 28 and 35 days of age. In addition, as described above, measurements were performed on samples that underwent thermal treatment at 28 days of age at temperatures 120 °C, 200 °C, 400 °C and 600 °C for 8 h at maximal temperature with a rate of heat 16 °C/min and free cooling down.

Effect of temperature on pore structure

Limitations of mercury intrusion porosimetry (MIP) measurements to quantify the actual pore size distribution of cementitious materials were discussed by Diamond[55]. To overcome some of these limitations, Kaufmann *et al.*[56] developed a multi-cycle MIP, which allows estimating the volume of ink-bottle pores.

In this study, multi-cycle MIP was performed on specimens of ages 3, 7 and 28 days, with or without thermal loading.

To evaluate the effect of thermal loading on porosity, samples were demolded at 28 days and crushed; corresponding chunks were subjected to designed thermal loads at 120 °C, 200 °C, 400 °C and 600 °C.

The raw data from mercury intrusion (volume of mercury versus applied pressure) was analyzed using the Washburn equation[57] for cylindrical pores to convert it into the equivalent pore size distribution. A surface tension of the mercury of 0.48 N/m^2 and a contact angle of 130° were assumed in the calculations.

To quantify the differences in the pore size distribution between the different mortars before and after thermal loading, besides the total porosity, also the breakthrough pore radius is analyzed. The breakthrough pore radius represents the minimum radius of pores that are percolated through the whole microstructure[58], and it has been related to transport properties of cementitious materials[59]. The breakthrough radius is found as the radius at which a sudden increase in intruded mercury volume is observed, and it can be conveniently identified as the first peak on the differential pore size distribution.

Coefficient of thermal expansion

The thermal expansion of the HPC-ref mix was measured with a thermal expansion dilatometer. Both the sample and reference material for the correction of thermal expansion were placed in the dilatometer. Change of length was recorded from 50 °C to the maximal temperature of 980 °C, with cooling down to 200 °C.

Expansion and shrinkage behavior was observed, and data is presented with correction for expansion of the system for the main HPC-ref matrix in Section 3.3. This data gives a basic overview of the main HPC-ref matrix used in this study.

3.3. RESULTS

Mechanical properties

Fig. 3.1 and Fig. 3.2 present data of elastic properties of the studied mortars after certain treatment. One can see the missing data for HPC-ref and HPC_SAP samples treated at 600 °C (Fig. 3.2). This is due to the actual spalling of the samples, making measurements of static Young's modulus following EN 12390-13 impossible. Where available, the error bars represent a standard deviation.

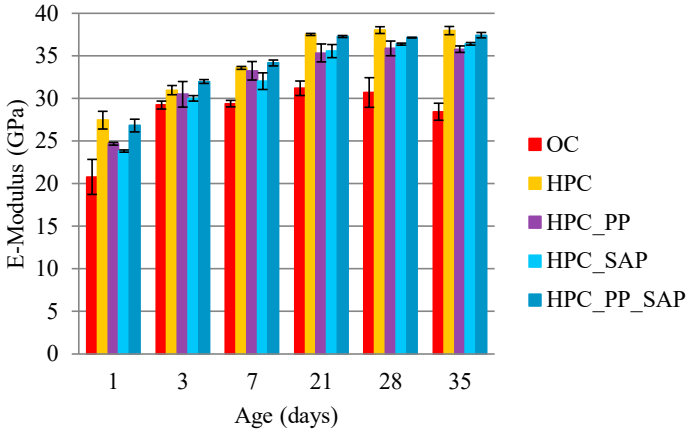

Fig. 3.1. Evolution of E-Modulus over time (samples stored at 20 °C with no thermal loading).

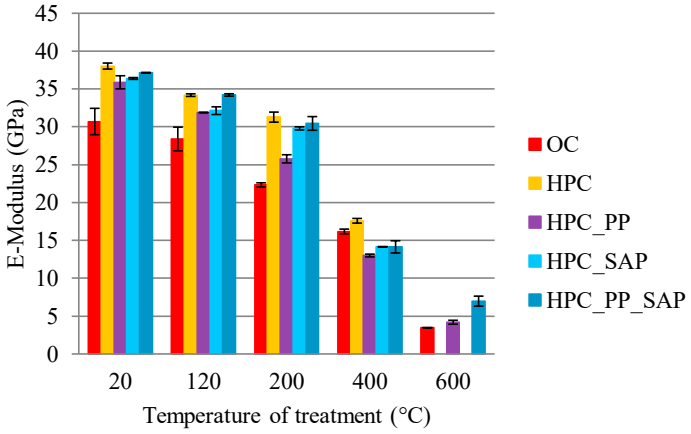

Fig. 3.2. Evolution of E-Modulus of samples at the age of 28 days due to thermal loads.

The following two figures (Fig. 3.3 and Fig. 3.4) present the result of compressive strength that was measured as well on the very same samples as static Young's modulus.

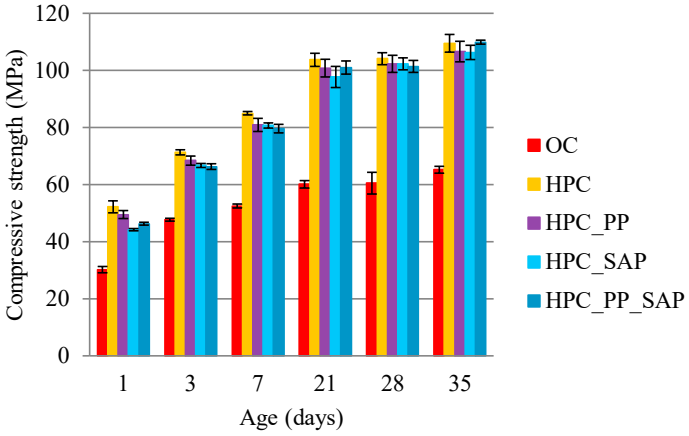

Fig. 3.3. Evolution of compressive strength over time.

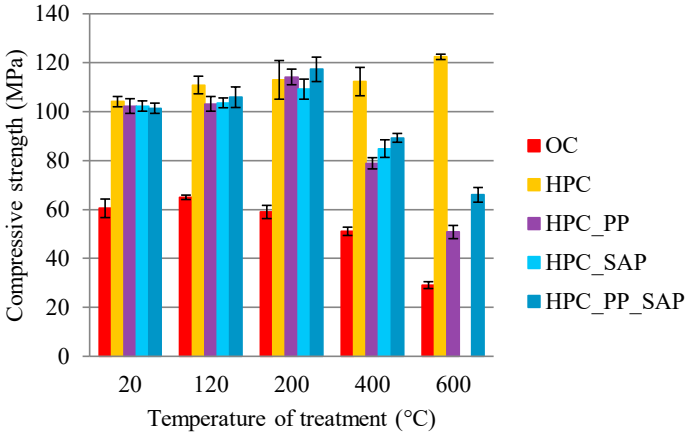

Fig. 3.4. Evolution of compressive strength of samples at the age of 28 days due to thermal loads.

Thermogravimetric Analysis

Here, results of TGA are presented in two ways: i) as general TGA curves for all 5 mixes where mass loss curves are a function of temperature, and ii) as mass loss after thermal loads. The focus is on mass loss, as it indicates the amount of moisture available at each step of thermal load. As a rough assumption, the mass loss before 600 °C is related to dehydration and loss of physically bound water, while mass loss above 600 °C is mainly due to decarbonation of carbonate phases (mainly calcium carbonate).

The TGA results of all 5 mixes at the age of 28 days are presented in Fig. 3.5.

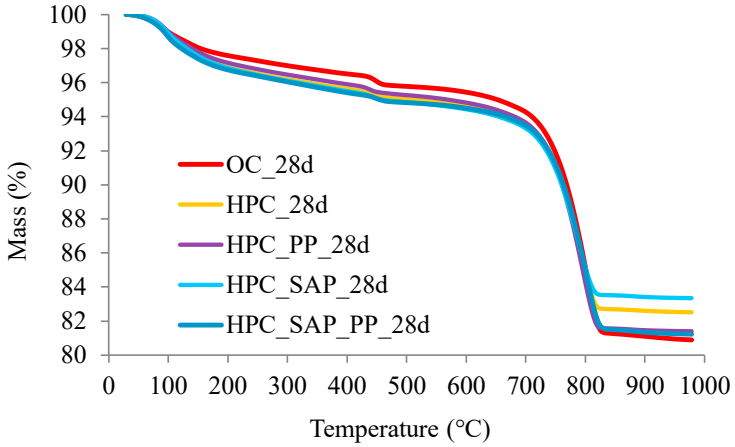

Fig. 3.5. TGA results of all the mixes at 28 days of age (samples cured at 20 °C without thermal loads).

Here we assume that no changes of carbonate phases take place during thermal loading of chunks at 120 °C, 200 °C, 400 °C, 600 °C and crop scale bar of temperature axis down to 600 °C, while we are mostly interested in the amount of H_2O available in the samples after thermal treatment and if rehydration of cement takes place. Once again, it is important to notice that data is presented for samples at the residual state after two cycles of solvent exchange.

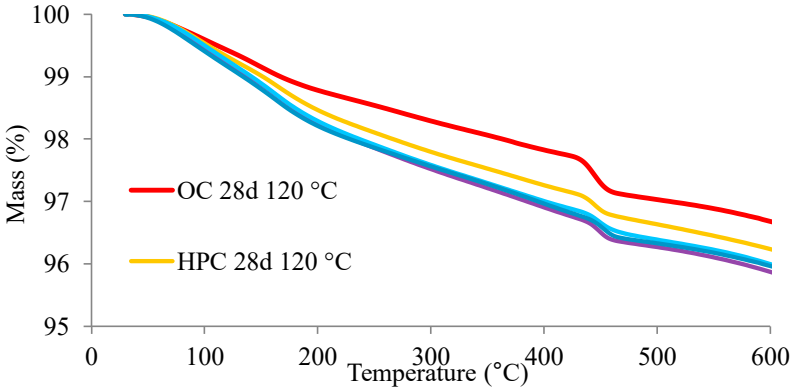

Fig. 3.6. TGA results of all the mixes at 28 days of age after treatment at 120 °C, the residual state.

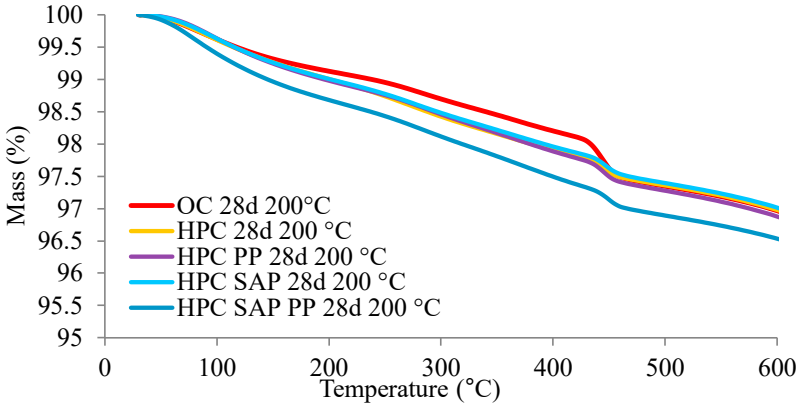

Fig. 3.7. TGA results of all the mixes at 28 days of age after treatment at 200 °C, the residual state.

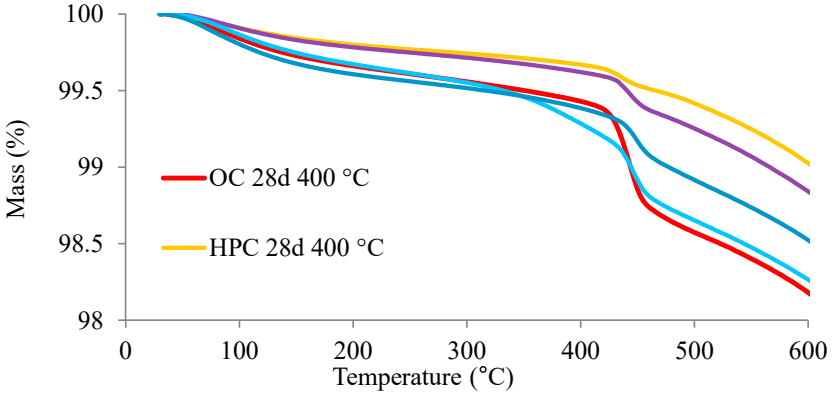

Fig. 3.8. TGA results of all the mixes at 28 days of age after treatment at 400 °C, the residual state.

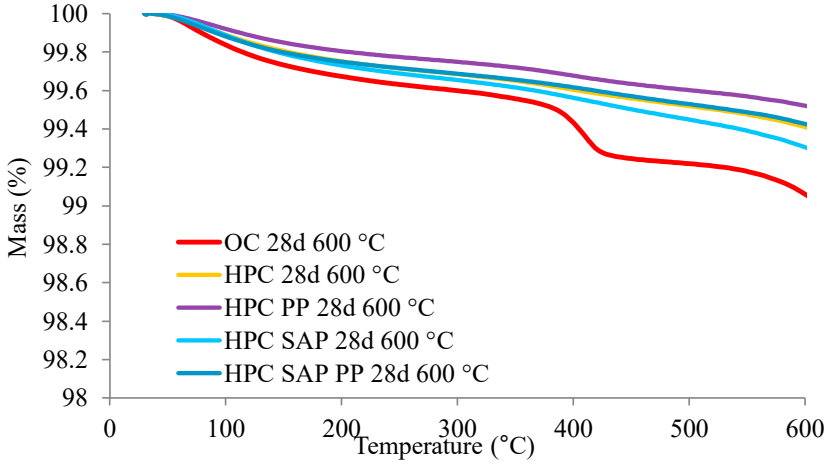

Fig. 3.9. TGA results of all the mixes at 28 days of age after treatment at 600 °C, the residual state.

Mercury Intrusion Porosimetry

A general type of data obtained with MIP is shown below on the OC sample at 28 days of hydration, see Fig. 3.10. Physical difference between the 1st cycle and the 2nd cycle is discussed in detail by Kaufmann[56]. Straightforward numerical value of the method provides the total porosity of the sample in percentage or mm^3/g; while the shape of the curve does not give us the pore size distribution[55, 56, 60, 61], it still provides valuable information on the breakthrough radius.

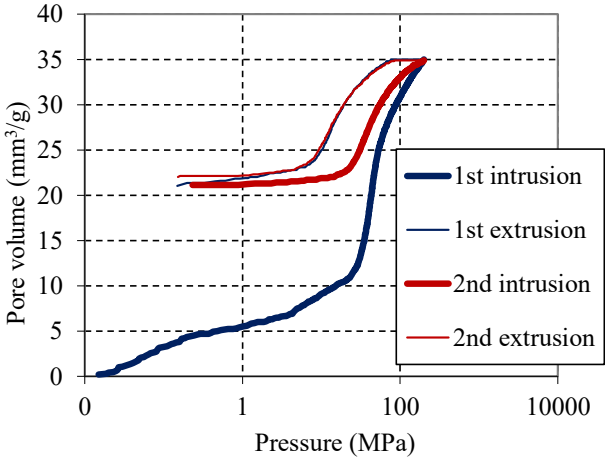

Fig. 3.10. Results of two-cycle MIP for OC sample at 28 days without thermal treatment.

Derivative of the data presented in Fig. 3.10 visualizes the breakthrough radius through which a large portion of pore volume is available, thus this radius is a threshold for transport properties and an example of a derivative curve for the OC sample at 28 days, presented in Fig. 3.11.

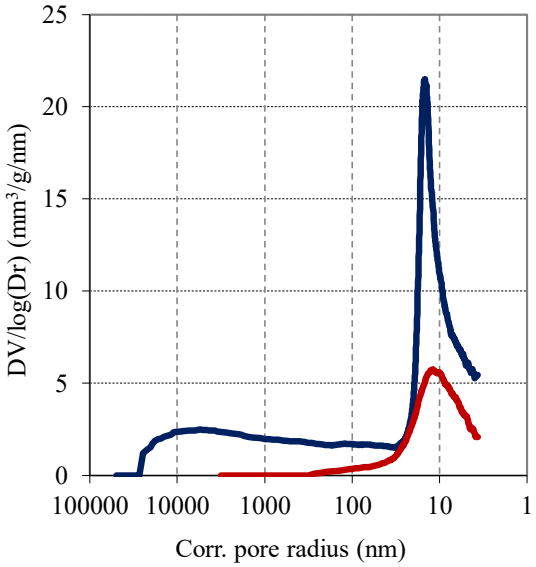

Fig. 3.11. Derivative curve of porosity, OC 28 days of age.

Results presented below summarize the peak values of the processed data, similar to the plots in Fig. 3.11 for all the samples. Evolution of total porosity and breakthrough radius over time, from time of mixing to the stop of hydration at 3, 7 and 28 days of age (Fig. 3.12 and Fig. 3.13 correspondingly). Fig. 3.14 and 3.15 present changes in total porosity and breakthrough radius for samples exposed to thermal loads of up to 600 °C at the age of 28 days.

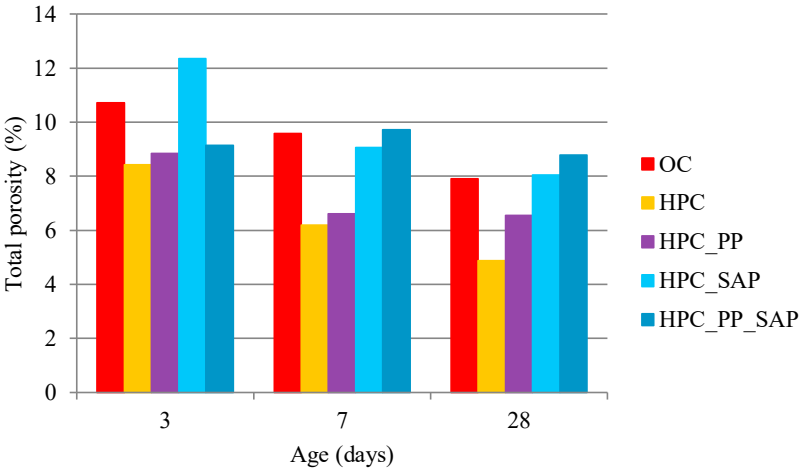

Fig. 3.12. Evolution of porosity due to hydration.

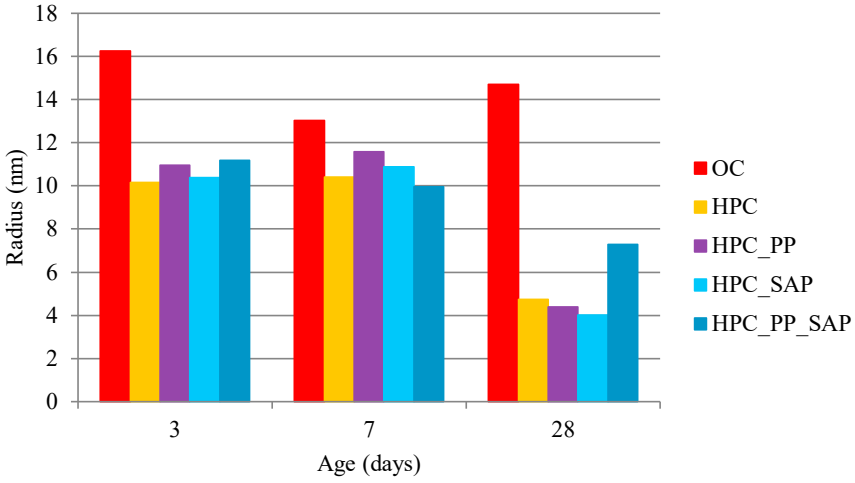

Fig. 3.13. Evolution of the breakthrough radius due to hydration.

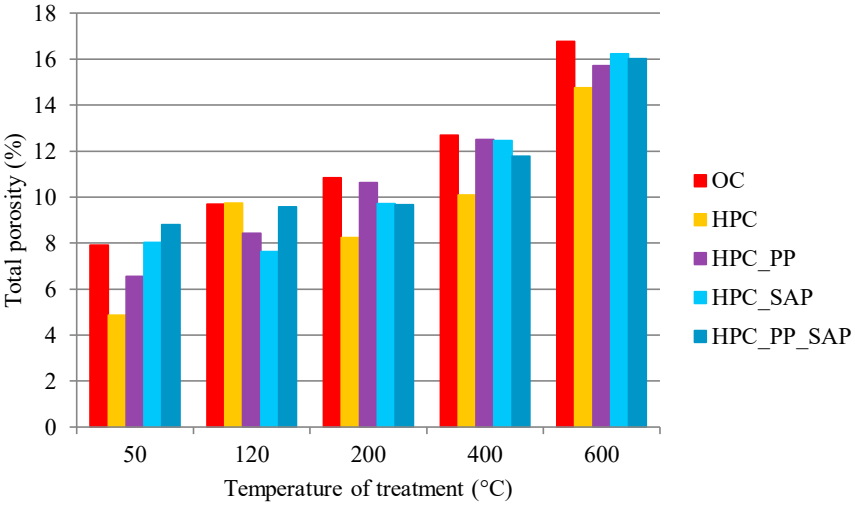

Fig. 3.14. Evolution of porosity at 28 days of age due to thermal loads.

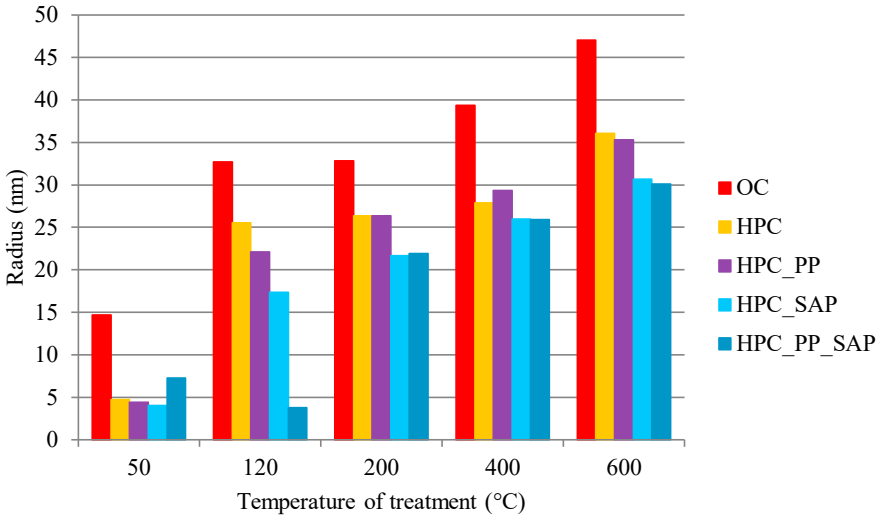

Fig. 3.15. Evolution of the breakthrough radius at 28 days of age due to thermal loads.

Thermal expansion

The curve of thermal expansion of the HPC main matrix is presented in Figure 3.16.

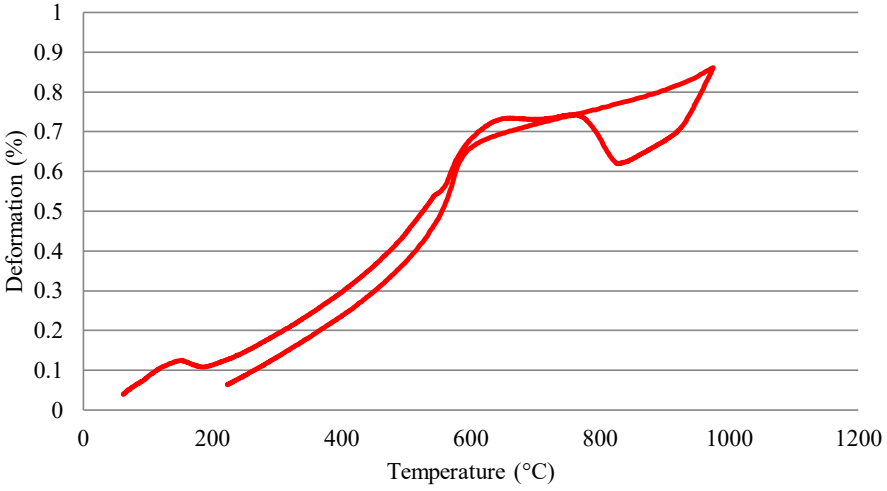

Figure 3.16. Thermal expansion of HPC mortar.

3.4.DISCUSSION

Complex and unified data on the residual state of material after exposure to elevated temperatures are presented in this chapter.

The residual mechanical properties measured in this study (see Fig. 3.2 and 3.4) are in good agreement with the literature overview (see Fig. 1.2 and 1.1 correspondingly).

The HPC samples for mechanical properties that spalled during thermal loading to 600 °C might have experienced a higher general damage; however, local damage of small pieces that were still eligible to perform compressive strength measurements on the same shape and at the same conditions showed twice as high compressive strength as those HPC+PP and HPC+PP+SAP samples that did not spall at 600 °C.

The breakthrough radius of HPC type mixes increases up to 6–7 times at 600 °C compared to thermally non-treated samples, while the same changes for OC samples are around ×3 the initial value (see Fig. 3.15). This indicates higher thermal damage done to high-performance concrete compared to ordinary concrete.

The pre-spalling state of material might have superior mechanical properties compared to one where the stresses are released uniformly due to having higher porosity, polymer fibers or SAP.

4. NONDESTRUCTIVE EVALUATION OF CONCRETE EXPOSED TO HIGH TEMPERATURES

4.1. APPLICATION OF NEUTRON RADIOGRAPHY TO CONCRETE

An effective method to measure water distribution in concrete is neutron radiography[62]. Research described in this chapter of the Thesis is a development of Weber *et al.*[63] study, eventually resulting in a number of papers[54, 64–68].

This research campaign resulted in both first ever visualized explosive spalling of concrete in 2D[64] and in 3D[68]. The author took part and produced all the specimens for two independent neutron imaging sessions, NEUTRA beamline[54, 64] at Paul Scherrer Institute (Villigen, Switzerland), and at NeXT D50 beamline[65–68] at Institute Laue-Langevin (Grenoble, France). The mix compositions used are identical, produced with the same equipment and mixing protocol. The datasets complement each other, and the microstructural study is presented in this Thesis.

Results and discussion

Fig. 4.1 a shows an X-ray radiograph of the sample that was acquired in order to determine the exact position of the thermocouples and of the pressure sensor heads. Fig. 4.1 b shows an exemplary neutron radiography image in which the drying front in the PP+SAP sample after 24 min of heating is evident. Some boundary effects are visible near the vertical edges of the sample due to imperfect insulation that led to faster drying. This effect can be attributed to both thermal insulation and moisture insulation. To exclude these boundary effects in the evaluation of the moisture profiles (see Fig. 4.4), only the region indicated by the rectangular frame in Fig. 4.1 b was considered for averaging the moisture content changes.

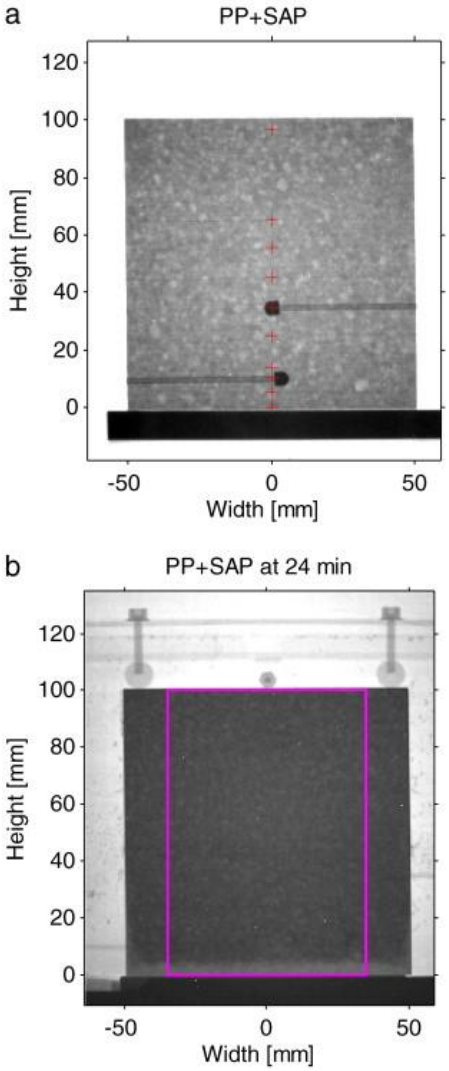

Fig. 4.1. a – X-ray raw radiography image showing the position of the thin thermocouples (indicated with crosses) and of the pressure sensor heads; b – neutron raw radiography image after 24 min of heating. The drying front is clearly visible. The rectangular contour in b indicates the averaging region for obtaining the moisture profile (Fig. 4.4). The gray levels refer to beam intensity[64].

As could be expected based on the findings presented in[69], the addition of both SAP and PP-fibers allowed avoiding spalling. On the other hand, spalling occurred after 24 min of heating in the sample with SAP only (Fig. 4.2). Spalling took the form of a large crack parallel to the heated surface along the whole length of the slab at a height of about 6 mm (corresponding to the position of the drying front, see Fig. 4.2 and 4.4 b).

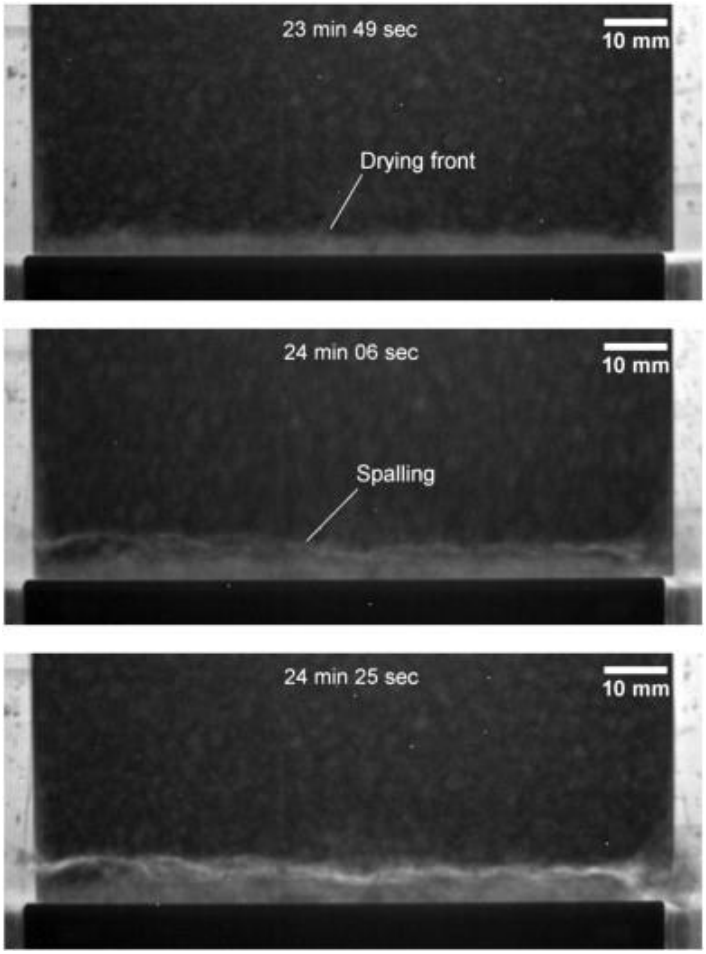

Fig. 4.2. Sequence of raw neutron radiographs (cropped bottom part of the sample) showing drying and spalling in the SAP mortar. Time 23:49 – just before spalling, the dried region is visible in brighter gray values. Time 24:06 – the spalling crack appears first as a fine line and widens in the successive radiographs. The gray levels refer to beam intensity[64].

The temperature profile was determined by fitting spline curves (Fig. 4.3) to the readings of the embedded thermocouples, whose locations were determined via X-ray radiography (Fig. 4.1 a). Note that the temperature at a height of 0 mm was assumed equal to the temperature of the copper block on which the sample was placed. Only the lower 35 mm near the heated surface is shown. There is no marked difference between the temperature profiles in the two samples, although the spatial resolution of the thermocouples is not fine enough for a precise assessment.

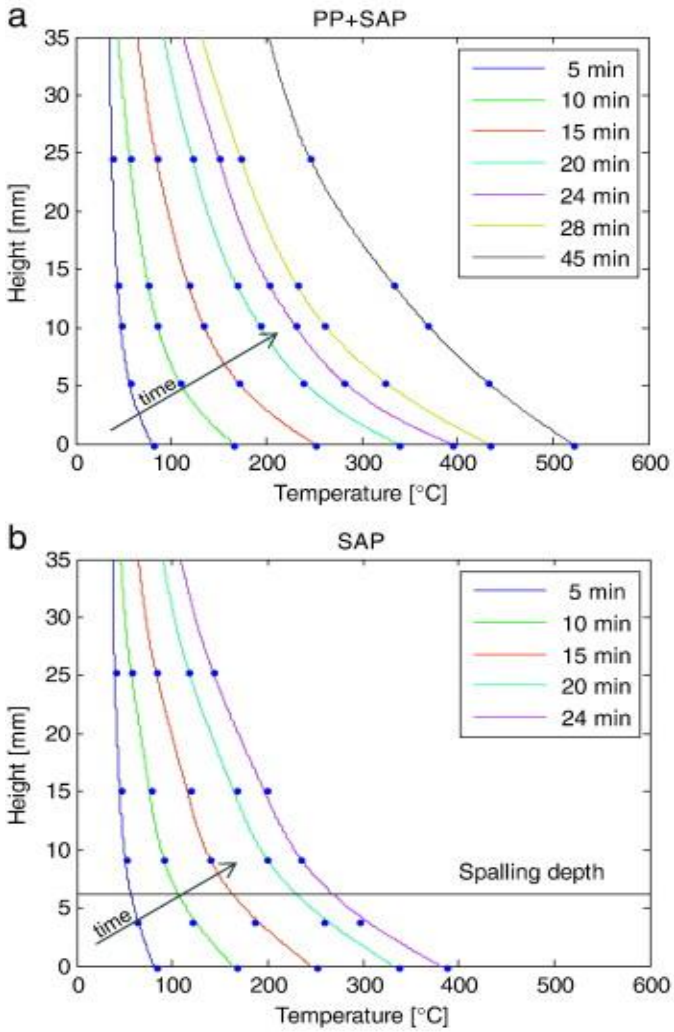

Fig. 4.3. Temperature profiles of the lower 35 mm of the mortar slab: a – PP+SAP sample (no spalling), and b – SAP sample (spalling occurred after 24 min at 6 mm height)[64].

The water loss profiles (expressed as equivalent water thickness[70, 71]) are shown in Fig. 4.4. The mixing water occupied approximately 20 % of the mortar volume (see Table 2.2), which, for a sample thickness of 25 mm, corresponds to an initial equivalent water thickness of 5 mm. The profiles were obtained by averaging at each height the change in moisture content along the horizontal line enclosed by the region indicated in Fig. 4.1 b. The profiles feature a plateau corresponding to a sudden change in slope where the water loss changes rapidly from almost zero to a large negative value over a small height. The approximate position (height) of the plateau, therefore, indicates the drying front, where a large portion of free and chemically bound

water disappears by vaporization and dehydration, respectively. Since the drying takes place in a certain narrow region, the plateau is not perfectly horizontal but extends over a certain height.

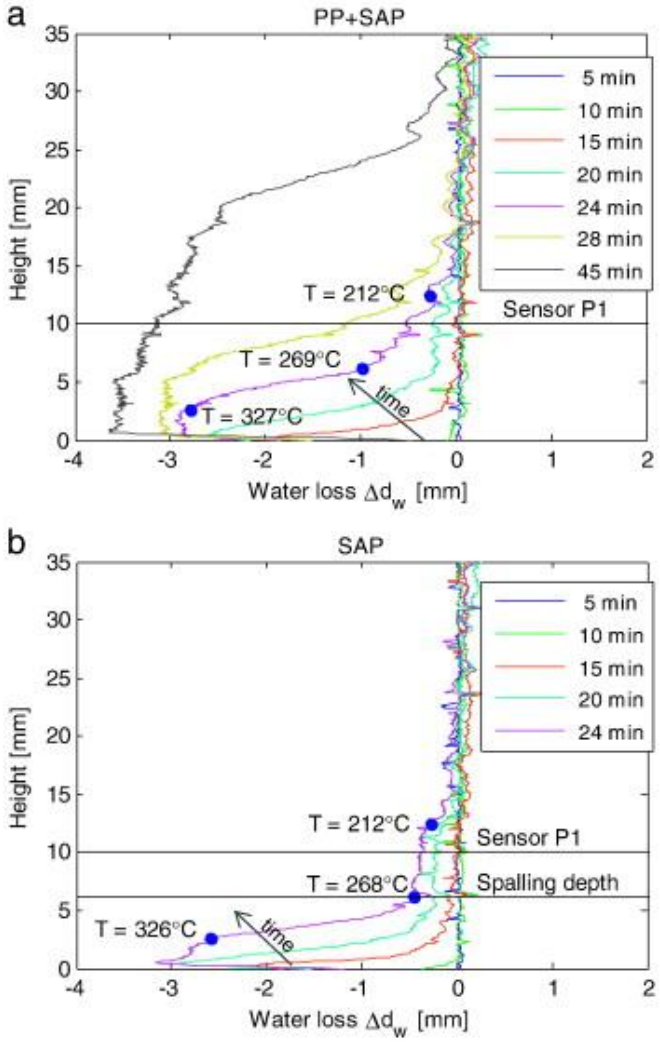

Fig. 4.4. Water loss profiles (expressed as equivalent thickness) of the lower 35 mm of the mortar slab (note that the profiles were measured for the whole height of the sample): a – PP+SAP sample (no spalling); b – SAP sample (spalling occurred after 24 min at 6 mm height). Estimated temperatures at 24 min are indicated for characteristic points of the profile[64].

The pore pressure measured by the pressure sensors (placed at 10 mm and 35 mm from the heated face) is shown in Fig. 4.5 as a function of time. The pressure peak is expected to be correlated to the drying front, where water loss proceeds at the highest rate. This is confirmed by the water loss profiles in the PP+SAP sample. It can be seen in Fig. 4.4 a, that the drying front (understood as the region where the moisture change profile shows a plateau) reaches the position of the first pressure sensor (located at 10 mm from the heated side) at about the same time when the maximum value of pressure is measured (compare the change of slope of the 28-

min profile at approximately 10 mm height in Fig. 4.4 a with the occurrence of the pressure peak at that time at the 10 mm position in Fig. 4.5 a).

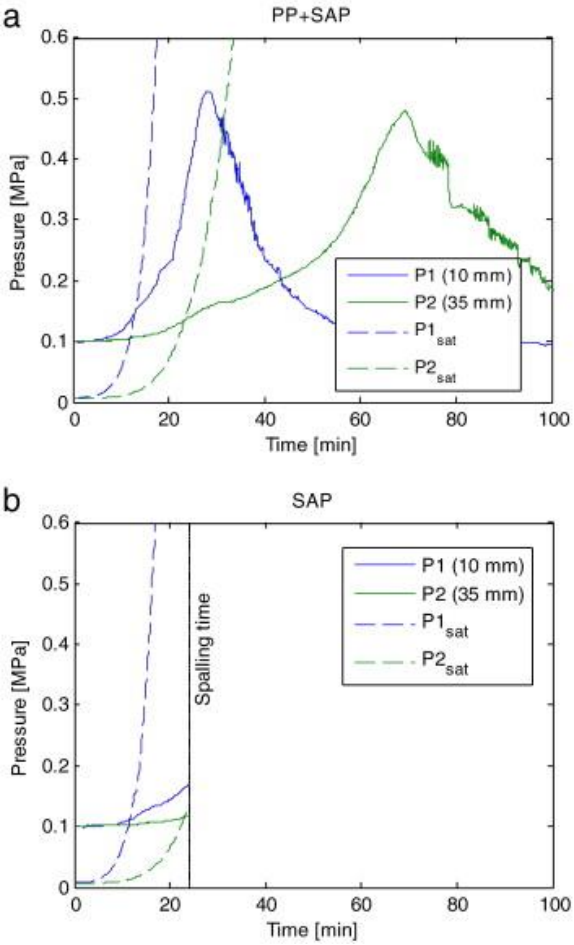

Fig. 4.5. Pore pressure measured by the two sensors P1 and P2 (nominal distance from the heated side indicated): a – PP+SAP sample (no spalling); b – SAP sample (spalling occurred after 24 min at 6 mm height). Vapor saturation pressure curves (calculated based on the temperature measured in correspondence with the sensors) are also reported[64].

The pressure in the sample with no PP-fibers (Fig. 4.5 a) is shown only up to the spalling event, since afterwards it is greatly influenced by the pressure release through the spalling crack. But even up to the spalling event, the pressure increases less than in the sample with PP-fibers (Fig. 4.5 a). This is consistent with the slower evolution of the drying front in the sample with no PP-fibers (Fig. 4.4 b), which suggests a slower advancement of the pressure peak and thus a larger distance from the pressure sensor at a given time (similar results were found by Kalifa *et al.*[72]).

4.1.1. Summary/conclusions

Neutron radiography has been performed on mortar slabs exposed to heating up to 550 °C, simultaneously monitoring temperature and pore pressure. The results obtained on two mortars with the same water-to-binder ratio equal to 0.34 are presented, the former with PP-fibers and SAP and the latter with SAP only. Since the addition of SAP leads to high moisture content, the risk of spalling is expected to increase with respect to HPC without internal curing. Spalling occurred in the mortar with SAP only in correspondence with the drying front at a temperature of approximately 260 °C. On the contrary, no spalling took place in the PP+SAP mortar. Thanks to the combined measurements of temperature, pore pressure and moisture distribution, the behavior of the mortars during heating has been investigated comprehensively. This approach is expected to provide new insight into the study of fire spalling mechanisms.

4.2. EVALUATION OF THERMALLY INDUCED DAMAGE WITH ULTRASOUNDS

4.2.1. Samples and protocol

This subsection aimed to characterize thermal cracking in normal (OC) and high-performance (HPC) concretes by means of ultrasonic (US) non-destructive methods, both linear and non-linear (two linear methods, pulse velocity (PV) and resonance ultrasonic spectroscopy (RUS), and a nonlinear ultrasonic technique, nonlinear resonant ultrasound spectroscopy (NRUS)). Additionally, the US methods aided with X-ray tomographies that are described in Section 4.3 of this Thesis were used. Measurements were performed on all mortar mixes presented in Table 2.2 of this Thesis: OC, HPC-ref, HPC+PP, HPC+SAP, HPC+PP+SAP, respectively. Two cylindrical mortar specimens of 100 mm in length and 25 mm in diameter were used for each mix composition. These three US measurement techniques were performed on the very same samples before thermal loading (virgin state) and after, thus enabling the exclusion of variations caused by the location of aggregates if physically different samples of the same mix were used.

For thermal loading, four temperatures were used:

T1 – 120 °C

T2 – 200 °C

T3 – 400 °C

T4 – 600 °C

A heating rate of 16.2 °C/min was chosen to agree with the rest of the tests with thermal loading. The maximal temperature was held for 8 hours, followed by free cooling down in the furnace for approximately 8 hours.

4.2.2. Results

Ultrasound pulse velocity

In Fig. 4.6, the effect of thermal treatment on ultrasonic pulse velocity is presented.

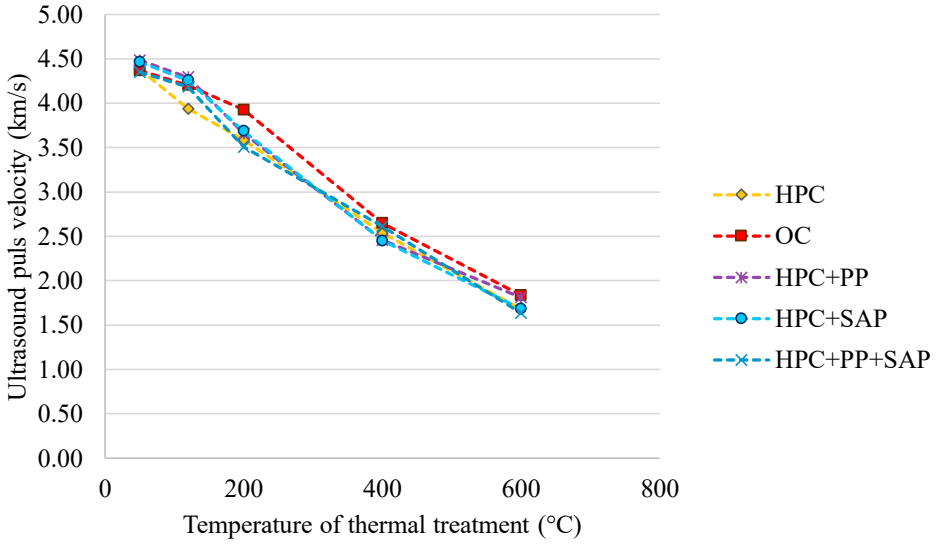

Fig. 4.6. Effect of thermal treatment on ultrasound pulse velocity.

Resonance ultrasound spectroscopy

Qualitative analysis of the RUS signal with RITA software gives general resonance peaks. Shift of longitudinal resonance frequency to the left can be seen in Fig. 4.7. Here, the author plots a limited signal frequency range for the sake of visualization of the data. The height (amplitude) of the peaks is not representative of a qualitative change within the material; it is mostly related to boundary conditions, e.g. contact between samples and transducers.

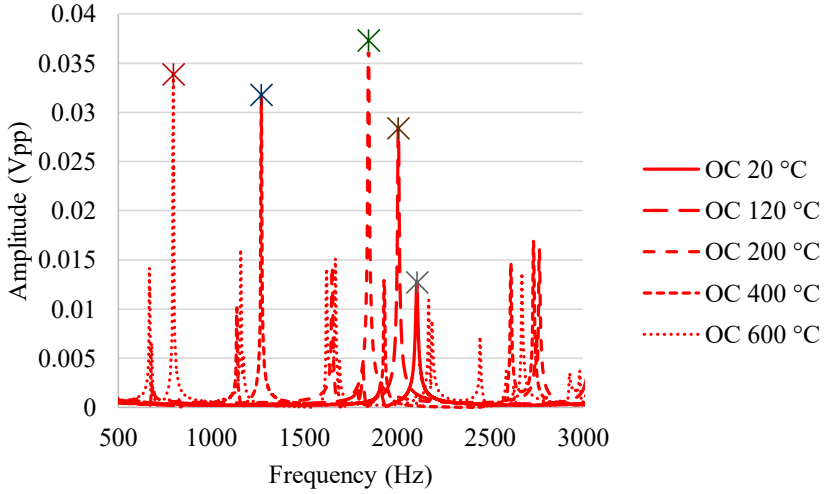

Fig. 4.7. RUS signal of thermally treated OC samples.

A general RUS data for HPC, similarly to OC (see Fig. 4.7), indicates a decrease of resonance frequency, e.g. shift to the left (see Fig. 4.8) after thermal loading.

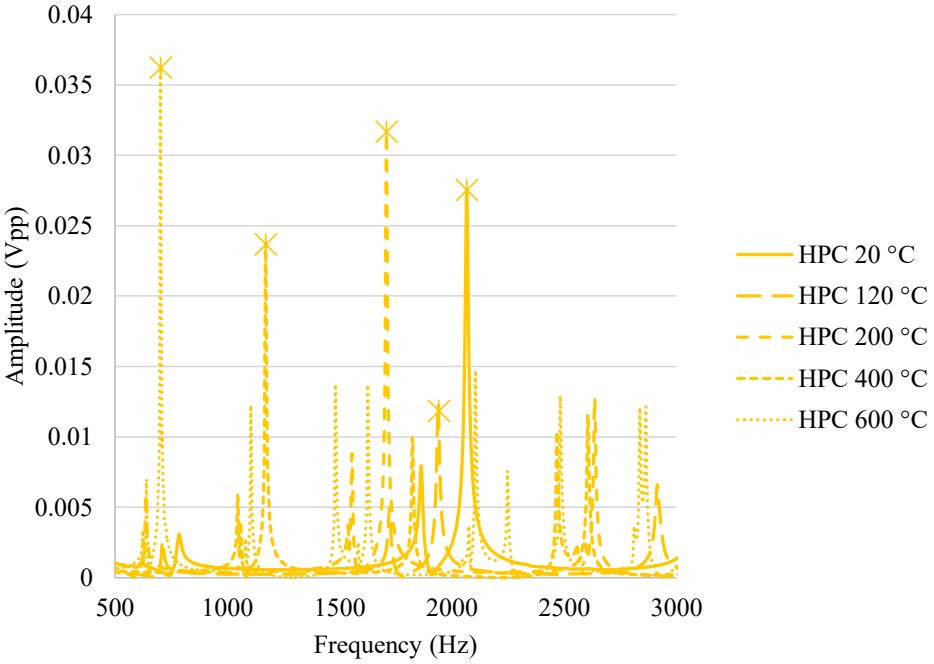

Fig. 4.8. RUS signal of thermally treated HPC samples.

RUS results of OC and HPC presented above are plotted for one single sample at each range of temperature. An evolution of residual dynamic Young's modulus for all the samples is presented in Fig. 4.9. All the samples without thermal load have a dynamic modulus in the range of 40–44 GPa.

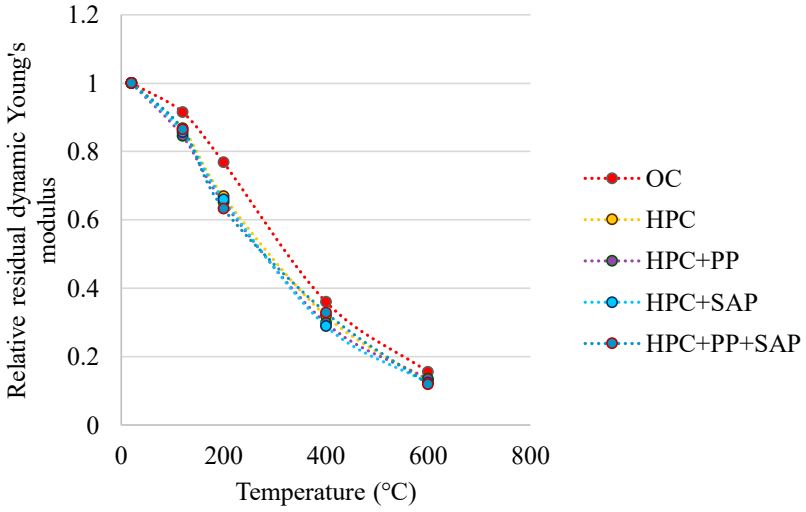

Fig. 4.9. Relative residual dynamic Young's modulus.

Nonlinear resonance spectroscopy

The linearity of the non-loaded samples is presented in a single figure (see Fig. 4.10), as all the NRUS signals of the samples from the same mix are averaged in a single curve. The linearity of the system is described by a sample of acrylic glass. As seen in Fig. 4.10, the most uniform sample is the reference of the system, the sample of the same geometry as the studied samples, made of acrylic glass. The least linear is the HPC sample.

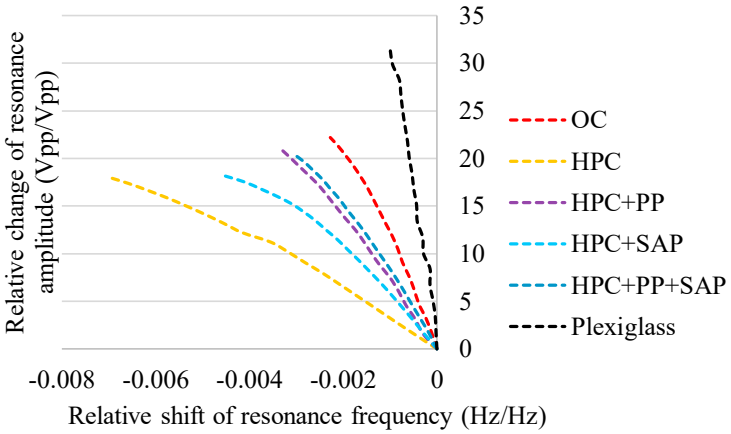

Fig. 4.10. Linearity of non-treated samples.

The set of figures below describes the linearity of samples after thermal treatment. The data for non-treated samples of OC and HPC are averaged from 8 samples, for the other three mixes, virgin linearity is an average of 4 samples. Results after thermal treatment are the average of two samples for OC and OPC, and results of one single sample for the other three mixes. Linearity of the system is described by a sample made of acrylic glass, as a reference.

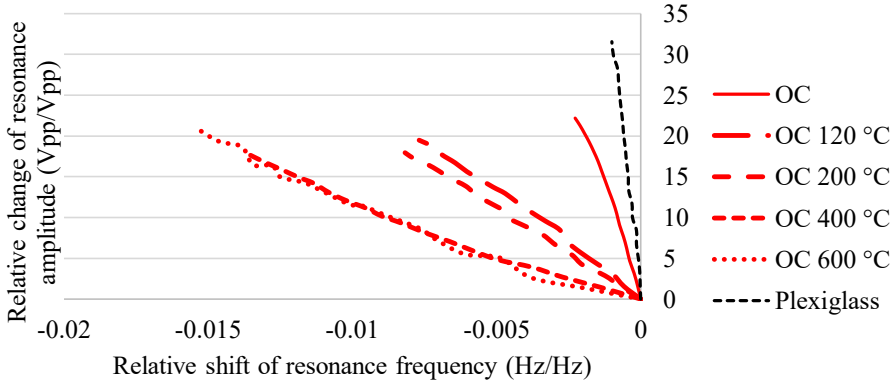

Fig. 4.11. Linearity of thermally treated OC samples.

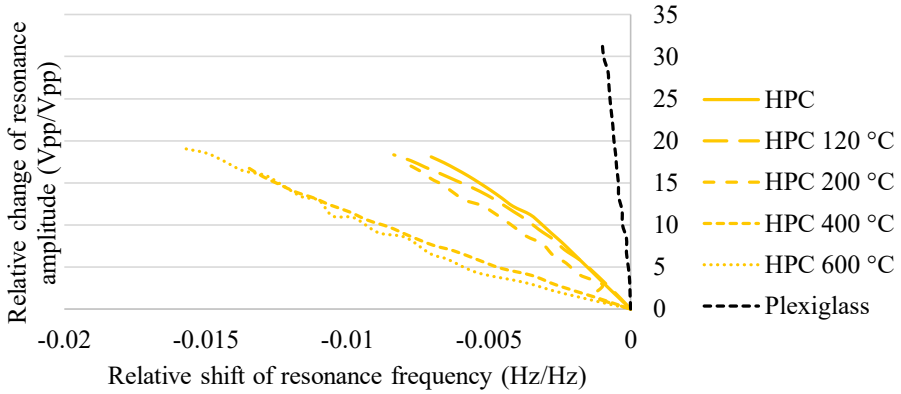

Fig. 4.12. Linearity of thermally treated HPC samples.

Table 4.1

Changes of Non-Linearity Coefficient α at High Temperatures

Mixes	Temperature of treatment				
	20 °C	120 °C	200 °C	400 °C	600 °C
OC	364.7	1089.5	1222.5	3380.0	4680.0
HPC	1216.1	967.0	1279.0	3142.5	5007.0
HPC+PP	601.8	964.0	1321.0	2824.0	15706.0
HPC+SAP	698.7	762.0	1228.0	2979.0	4505.0
HPC+PP+SAP	656.3	707.0	1468.0	3079.0	4590.0

4.2.3. Discussion

Experimental data obtained in this study are plotted as relative residual UPV and compared with the literature data presented in Section 1.2 of this Thesis (see Fig. 4.13).

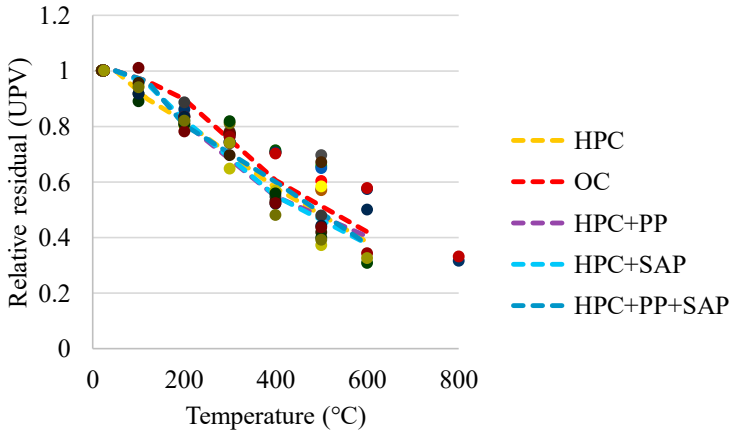

Fig. 4.13. Comparison of experimental UPV data with literature data.

Experimental data follow the general trend seen in literature, indicating deterioration of the elastic properties of concrete at high temperatures. The initial UPV of all 5 mixes is in the range 4.35 km/s to 4.5 km/s, which is about 10 % lower than the samples studied by Sultan[23], Eidan[25] and Kim[27].

The presence of empty volumes initially created by SAP is not affecting the evolution of residual UPV significantly; one could compare those artificially created cavities with ultra-light aerogel incorporations.

To follow the data, one has to take into account that UPV is a linear function of Young's modulus. The decrease of UPV over temperatures seems linear, e.g. decrease of Young's modulus; however, different processes are behind this decrease. The initial decrease at temperatures below 100 °C should mostly be due to direct loss of moisture, and no significant thermal damage is expected. At the range 100–200 °C, two types of changes take place, both decomposition of hydration products (e.g. ettringite) and possibly formation of new hydration products in the ITZ zone. The dehydration process is more global and affects the whole sample, while solidification in the ITZ zone is local and affects UPV less than a dehydration of a straight pass for the US through the paste. To visualize the local effects, nonlinear US methods like SIMONRUS (Single Mode Nonlinear Resonance Ultrasound Spectroscopy) are of interest.

Results of RUS indicate a uniform decrease of dynamic Young's modulus (see Fig. 4.9) similar to static Young's modulus (Fig. 3.2). However, compared to the study of static modulus, no samples experienced explosive spalling, and all were available for measurements.

Very limited data on the evaluation of nonlinearity of the thermally damaged concrete samples can be found in the literature; temperature change during the measurements is a known source of measurement error[75], and thus performance of the hot test is a challenge. Application of nonlinear ultrasound methods can be carried out on the samples in a residual state, the general range of obtained α is in good agreement with literature data, where Payan *et al.*[74] reported α values for samples treated at 120 °C as 1204 and 966 for OC and HPC, respectively. The corresponding values in this study are 1089.5 and 967, respectively.

No effect of temperature fluctuation during NRUS measurements was observed by means of an infrared thermal camera; this can be attributed to sample size, low driving amplitudes and use of the Haupert protocol[75].

These results are very promising and highlight the power of combined linear and nonlinear US methods for evaluating thermal damage of concrete. However, deeper investigation of shrinkage-induced cracking, healing of the cracks and changes in the ITZ zone at the lower (up to 200 °C) temperatures are of interest.

Besides the investigation of micro damage by means of US techniques, the close to linear correlation between the residual UPV and the temperature to which the samples were exposed is observed. This has a high practical application to post factum determining the actual temperature of a concrete structure during a fire event, where the UPV measurements can be performed on potentially damaged parts of the structure and the part of the structure of the same concrete mix, which had no exposure to fire. This comparison of residual UPV would provide both information on the potential scale of damage and map the area that had been exposed to high temperatures, indicating the “hot spots” of the event.

Additionally, the cores can be taken for mechanical tests, as the results of static elastic modulus, in general, follow the linear trend versus temperatures of exposure. The result of compressive strength shows less of a linear trend.

4.2.4. Summary/conclusions

At the lower temperatures or a very short-term thermal exposure, local changes of the solid HPC matrix can increase linearity of the material, thus almost providing a beneficial effect.

Practical application of UPV measurements can mislead the user, as a drop in UPV does not directly mean a drop in mechanical properties.

The obtained NRUS data support the hypothesis of further hydration at ITZ zones and healing of microcracks induced originally by autogenous shrinkage during hardening and/or drying shrinkage at temperatures up to 200 °C.

4.3. EVALUATION OF THERMALLY INDUCED DAMAGE WITH µCT

4.3.1. Samples and protocol

Physically, the same samples were used for µCT study of thermally induced damage as for the US campaign; however, no duplicates for each range of temperatures, unlike for the US-measurements.

4.3.2. Methods

Full rotation protocol with steps of 0.5° and 721 radiographs in total were recorded for each µCT dataset. The distance from the source to the detector was set at 1016 mm, with a detector size of 1024 × 1024 pixels and the conical beam source. The current of 140 uA and voltage of 70 kV were used for samples before thermal treatment; corresponding values for thermally loaded samples were 140 uA and 100 kV. A dataset with a pixel size of 0.02659 mm and the same distance between slices was recorded, resulting in a voxel size of 18.8×10^{-6} mm.

Empa's Image Analysis Platform was used for reconstruction, registration and processing of the data. Octopus software was used for reconstruction, while 2D registration and different plugins, including rendering of 3D View, were done in Fiji/ImageJ. The calculations were performed on 8-bit images, dividing material compounds into clusters based on gray levels. A similar approach was used to study the interface between opalinus clay and concrete[81].

Most of the thermal damage was observed in sub-pixel scale, thus the opportunity for a quantitative, reliable 3D rendering of cracks was limited. However, qualitative analysis of the obtained data is discussed below.

4.3.3. Results

Processing of post- and pre- thermally treated µCT data allows us to observe qualitative changes and thermal cracking in different temperature steps. It is important to notice that every

μCT of a thermally loaded sample has the μCT data of the very same sample before thermal loading, thus the actual damage can be visualized.

An example of volumetric distribution of air bubbles in OC and HPC is given in Fig. 4.14 and Fig. 4.15, respectively.

Table 4.2

Volumetric Content of Voids, Calculated from μCT

Mix	Volume of voids, %
OC	2.47
HPC	4.42
HPC+PP	3.31
HPC+SAP	5.11
HPC+PP+SAP	5.1

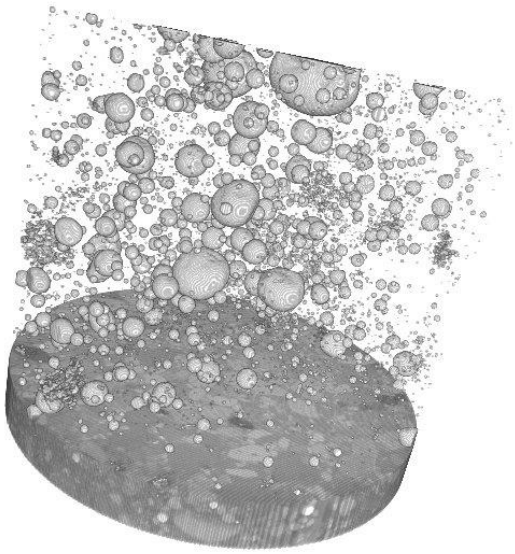

Fig. 4.14. Visualization of air bubbles for the OC T1-1 sample before thermal treatment.

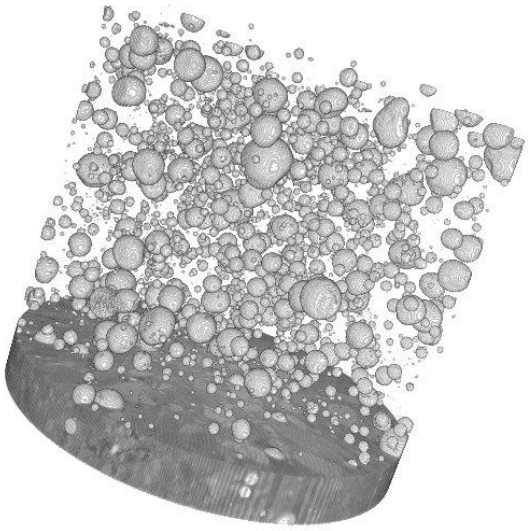

Fig. 4.15. Visualization of air bubbles for the HPC T1-1 sample before thermal treatment.

It has to be noted that the volumetric content of voids presented above does not directly mean the air content, as some small air bubbles might not be resolved or visualized after reconstruction, registration and correction for beam hardening artefacts, as voxel size is below 18.8×10^{-6} mm^3.

The qualitative evaluation of thermal damage of HPC samples at 600 °C is presented in Fig. 4.16.

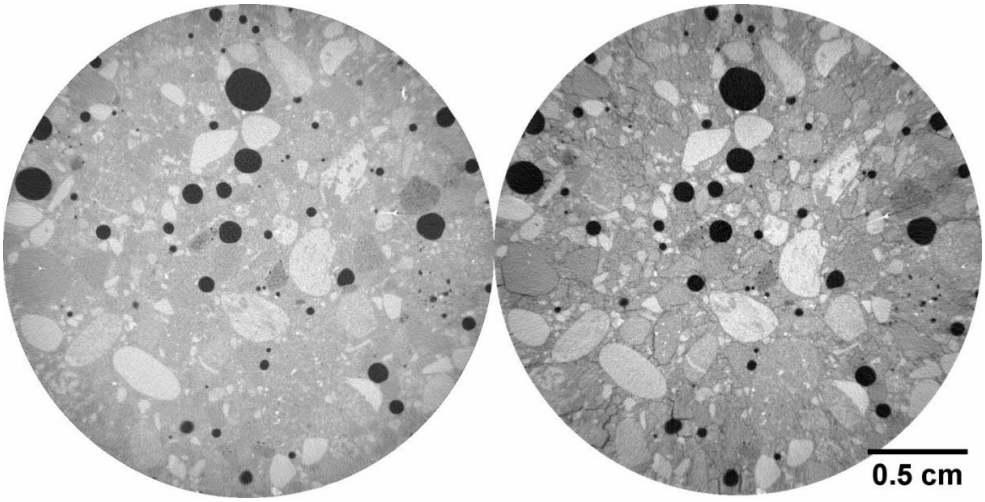

Fig. 4.16. Thermal damage of HPC at 600 °C: left – before thermal load; right – after thermal load.

4.3.4. Summary/conclusions

Nondestructive test methods, like X-ray tomography, are of high value in qualitative analysis of the state of the material. This allows to visualize the damage and to localize the initial damage, both volume and temperature/time-wise.

No obvious cracks were observed at temperatures of 120 °C and 200 °C, while at 600 °C, HPC experienced severe cracking.

The obtained μCT data highlight the positive effect of SAP and PP on the restriction of thermal damage to concrete, where very limited cracking is observed for samples with SAP and PP, compared to plain HPC samples.

5. CONCLUSIONS

Both the literature review and the study of properties of mortars after thermal loads indicate a possible increase in mechanical properties at temperatures around 200 °C, a general decrease above 400 °C and deterioration of residual compressive strength for samples loaded above 800°C. As for the case of samples tested here, the highest increase in compressive strength after thermal treatment was achieved for HPC samples at 600 °C, and it was +17.58 %; however, the sample itself experienced spalling, and this indicates only the potential of the material. The highest increase in bending strength was for HPC+PP+SAP samples after 200 °C treatment, which resulted in +18.49 %. The highest relative deterioration in compressive and flexural strength was recorded for OC samples at 600 °C, –51.90 % and –81.32 %, respectively. It is here to mark that samples with only PP fibers added experienced higher drop in strength than HPC samples (–50.34 % compressive and –67.23 % flexural), however when SAP was introduced to the mixture, the relative decrease in strength was more moderate (–34.91 % compressive and –49.58 % flexural), but could lead to a spalling at high temperatures due to higher water content, that correlates with the neutron radiography study.

The total porosity and breakthrough radius measured by means of MIP both showed an increase over temperatures of loading. The total porosity for OC samples after thermal loading at 600 °C increased 2.12 times, while for the HPC sample, the total porosity increased 3.03 times, indicating higher damage. It is important that the smallest increase after thermal loading to 600 °C had HPC+PP+SAP samples.

This data is supported by a general increase in residual transport properties measured by means of oxygen diffusion. The highest increase in transport properties based on oxygen diffusion was observed for HPC samples at 400 °C, which increased 122.21 times, indicating the damage. At higher temperatures, the damage was even more significant, as the equipment went out of range and the state of the samples often could not be expressed numerically.

Spalling is likely to occur for HPC mixes exposed to high temperatures. Pressure generated by water vapor and thermal stress combined can lead to explosive spalling. It is important to keep in mind that explosive spalling is not a property of material but a complex combination of factors that lead to certain behavior of a structure experiencing thermal loads.

Neutron radiography has been performed on mortar slabs exposed to heating up to 550 °C, simultaneously monitoring temperature and pore pressure. The results obtained on two mortars with the same water-to-binder ratio equal to 0.34 are presented: the former with PP-fibers and SAP and the latter with SAP only. Since the addition of SAP leads to high moisture content, the risk of spalling is expected to increase with respect to HPC without internal curing. Spalling occurred in the mortar with SAP only in correspondence with the drying front at a temperature of approximately 260 °C. On the contrary, no spalling took place in the PP+SAP mortar. Thanks to the combined measurements of temperature, pore pressure and moisture distribution, the behavior of the mortars during heating has been investigated comprehensively. This approach provides new insight into the study of fire spalling mechanisms.

The comparison between the moisture profiles and the pressure development allows inferring that the peak pressure occurs within the drying front. Thus, the more localized and more slowly advancing drying front observed in the sample without PP-fibers supports also a narrower pressure peak, which develops closer to the heated face.

Sufficient thermal insulation and aluminum shielding are able to protect the scintillator from high temperatures and spalling of concrete placed just a few centimeters away from it, as the close distance is required for better resolution. The experiments described in this Thesis set a path for further studies of spalling by means of neutron radiography.

The non-destructive US methods indicated a clear decrease in residual Young's modulus at each step of thermal loads, with only 15.53 % of dynamic Young's modulus left for OC samples, 13.12 % for HPC samples, HPC+PP – 14.09 %, HPC+SAP – 12.32 %, HPC+PP+SAP – 11.94 %. While analysis of NRUS data supports the idea of local healing of shrinkage cracks for HPC and HPC+PP samples, and solidification of the ITZ zone.

The important practical conclusion of this work is the linear trend observed for residual UPV over the increase of temperatures. The clear, close to linear, decline of residual UPV allows by comparing conditions of structure at different points to draw conclusions about the maximal temperature the structural elements were exposed to.

The qualitative data obtained by x-ray μCT, besides the cracking, generally visualizes that cracks are more likely to form around softer aggregates than denser ones.

The study presented here is the first effort to combine a number of non-destructive methods to evaluate damage in concrete due to high temperatures, which was done consistently and based on a uniform set of samples.

REFERENCES

1. Damtoft, J. S., Lukasik, J., Herfort, D., Sorrentino, D., & Gartner, E. M. Sustainable development and climate change initiatives. *Cem. Concr. Res.* **38**, 115–127 (2008).
2. Barcelo, L., Kline, J., Walenta, G., & Gartner, E. Cement and carbon emissions. *Mater. Struct. Constr.* **47**, 1055–1065 (2014).
3. Monteiro, P. J. M., Miller, S. A., & Horvath, A. Towards sustainable concrete. *Nat. Mater.* **16**, 698–699 (2017).
4. Kalifa, P., Menneteau, F. D., & Quenard, D. Spalling and pore pressure in HPC at high temperatures. *Cem. Concr. Res.* **30**, 1915–1927 (2000).
5. Flatt, R., & Schober, I. Superplasticizers and the rheology of concrete. in *Understanding the Rheology of Concrete* 144–208 (Woodhead Publishing Limited, 2012). doi:10.1533/9780857095282.2.144
6. Neville, A., & Aïtcin, P.-C. High performance concrete- An overview. *Mater. Struct.* **31**, 111–117 (1998).
7. European Commission. *Competitiveness of the European Cement and Lime Sectors*. (2017).
8. Mindeguia, J.-C., Pimienta, P., Noumowé, A., & Kanema, M. Temperature, pore pressure and mass variation of concrete subjected to high temperature – Experimental and numerical discussion on spalling risk. *Cem. Concr. Res.* **40**, 477–487 (2010).
9. Ulm, F., Acker, P., & Levy, M. The "Chunnel" fire. II: Analysis of concrete damage. *J. Eng. Mech.* **125**, 283–289 (1999).
10. Khoury, G. A. Effect of fire on concrete and concrete structures. *Prog. Struct. Eng. Mater.* **2**, 429–447 (2000).
11. Kodur, V. Spalling in high strength concrete exposed to fire: concerns, causes, critical parameters and cures. *Adv. Technol. Struct. Eng.* 1–9 (2000).
12. Ulm, F. J., Coussy, O., & Bažant, Z. P. The 'Chunnel' fire. I: Chemoplastic softening in rapidly heated concrete. *J. Eng. Mech.* **125**, 272–281 (1999).
13. Jansson, R. Fire spalling of concrete: theoretical and experimental studies. (2013). doi:1103-4270
14. *EN 1992-1-2. Eurocode2: General rules – Structural fire design*.
15. Ingason, H., Li, Y. Z., & Lönnermark, A. Runehamar tunnel fire tests. *Fire Saf. J.* **71**, 134–149 (2015).
16. Lönnermark, A., & Ingason, H. Gas temperatures in heavy goods vehicle fires in tunnels. *Fire Saf. J.* **40**, 506–527 (2005).
17. Lönnermark, A., & Ingason, H. Fire spread and flame length in large-scale tunnel fires. *Fire Technol.* **42**, 283–302 (2006).
18. Ingason, H., & Lönnermark, A. Heat release rates from heavy goods vehicle trailer fires in tunnels. *Fire Saf. J.* **40**, 646–668 (2005).
19. ITA. *Guidelines for structural fire resistance for road tunnels*. (2004).
20. Dong, Y. *et al.* Experimental research on fire resistance of the reduced scale immersed tunnel with fire in both traffic tubes. *Tunn. Undergr. Sp. Technol.* **132**, 104922 (2023).
21. Felicetti, R., & Gambarova, P. G. Effects of High Temperature on the Residual Compressive Strength of High- Strength Siliceous Concretes. *ACI Mater. J.* **95**, (1998).
22. Canbaz, M. The effect of high temperature on reactive powder concrete. *Constr. Build. Mater.* **70**, 508–513 (2014).

23. Sultan, H. K., & Alyaseri, I. Effects of elevated temperatures on mechanical properties of reactive powder concrete elements. *Constr. Build. Mater.* **261**, 120555 (2020).
24. Alimrani, N. S., & Balazs, G. L. Synthetic fibres or fibre cocktail in terms of shear capacity of concrete after elevated temperatures. *Mech. Mater.* **148**, 103504 (2020).
25. Eidan, J., Rasoolan, I., Rezaeian, A., & Poorveis, D. Residual mechanical properties of polypropylene fiber-reinforced concrete after heating. *Constr. Build. Mater.* **198**, 195–206 (2019).
26. Abaeian, R., Behbahani, H. P., & Moslem, S. J. Effects of high temperatures on mechanical behavior of high strength concrete reinforced with high performance synthetic macro polypropylene (HPP) fibres. *Constr. Build. Mater.* **165**, 631–638 (2018).
27. Kim, Y. S., Ohmiya, Y., Kanematsu, M., & Kim, G. Y. Effect of aggregate on residual mechanical properties of heated ultra-high-strength concrete. *Mater. Struct. Constr.* **49**, 3847–3859 (2016).
28. Liu, J. C. & Tan, K. H. Fire resistance of ultra-high performance strain hardening cementitious composite: Residual mechanical properties and spalling resistance. *Cem. Concr. Compos.* **89**, 62–75 (2018).
29. Irshidat, M. R., Al-Nuaimi, N., & Rabie, M. Hybrid effect of carbon nanotubes and polypropylene microfibers on fire resistance, thermal characteristics and microstructure of cementitious composites. *Constr. Build. Mater.* **266**, 121154 (2021).
30. Beaucour, A. L. *et al.* Influence of elevated temperature on properties of radiation shielding concrete with electric arc furnace slag as coarse aggregate. *Constr. Build. Mater.* **256**, 119385 (2020).
31. Algourdin, N., Sy Hung, B., Mesticou, Z., & Si Larbi, A. Effects of high temperature on mechanical behaviour and physicochemical properties of recycled mortars and its components. *Constr. Build. Mater.* **248**, 118554 (2020).
32. Nayel, I. H., Nasr, M. S., & Abdulridha, S. Q. Impact of elevated temperature on the mechanical properties of cement mortar reinforced with rope waste fibres. *IOP Conf. Ser. Mater. Sci. Eng.* **671**, 0–10 (2020).
33. Papayianni, J., & Valiasis, T. Residual mechanical properties of heated concrete incorporating different pozzolanic materials. *Mater. Struct.* **24**, 115–121 (1991).
34. Saedi Daryan, A., Bakhtiari, M., & Ghasemi, P. An experimental study to evaluate the postfire mechanical properties of concrete specimens. *Struct. Concr.* 1–13 (2020). doi:10.1002/suco.202000011
35. Niknezhad, D., Bonnet, S., Leklou, N., & Amiri, O. Effect of thermal damage on mechanical behavior and transport properties of self-compacting concrete incorporating polypropylene fibers. *J. Adhes. Sci. Technol.* **33**, 2535–2566 (2019).
36. Chang, Y. F., Chen, Y. H., Sheu, M. S., & Yao, G. C. Residual stress-strain relationship for concrete after exposure to high temperatures. *Cem. Concr. Res.* **36**, 1999–2005 (2006).
37. Noumowe, A. N., Clastres, P., Debicki, G., & Costaz, J. L. Transient heating effect on high strength concrete. *Nucl. Eng. Des.* **166**, 99–108 (1996).
38. Zhai, Y., Deng, Z., Li, N., & Xu, R. Study on compressive mechanical capabilities of concrete after high temperature exposure and thermo-damage constitutive model. *Constr. Build. Mater.* **68**, 777–782 (2014).
39. Zheng, W., Li, H., & Wang, Y. Compressive stress-strain relationship of steel fiber-reinforced reactive powder concrete after exposure to elevated temperatures. *Constr.*

Build. Mater. **35**, 931–940 (2012).
40. Chan, Y. N., Peng, G. F., & Anson, M. Residual strength and pore structure of high-strength concrete and normal strength concrete after exposure to high temperatures. *Cem. Concr. Compos.* **21**, 23–27 (1999).
41. Phan, L. T., Lawson, J. R., & Davis, F. L. Effects of elevated temperature exposure on heating characteristics, spalling, and residual properties of high performance concrete. *Mater. Struct. Constr.* **34**, 83–91 (2001).
42. Lau, A., & Anson, M. Effect of high temperatures on high performance steel fibre reinforced concrete. *Cem. Concr. Res.* **36**, 1698–1707 (2006).
43. Xuan, W., Chen, X., Yang, G., Dai, F., & Chen, Y. Impact behavior and microstructure of cement mortar incorporating waste carpet fibers after exposure to high temperatures. *J. Clean. Prod.* **187**, 222–236 (2018).
44. Collier, N. C. Transition and decomposition temperatures of cement phases – a collection of thermal analysis data. *Ceram. – Silikaty* **60**, 338–343 (2016).
45. Jiang, C., Fang, J., Chen, J. Y., & Gu, X. L. Modeling the instantaneous phase composition of cement pastes under elevated temperatures. *Cem. Concr. Res.* **130**, 105987 (2020).
46. Shorter, G. W., & Harmathy, T. Z. Discussion of the fire resistance of prestressed concrete beams. In: *Proceedings of the Institution of Civil Engineers,* 313–315 (1961).
47. Saito, H. Explosive Spalling of Prestressed Concrete in Fire. *Bull. Japan Assoc. Fire Sci. Eng.* **5**, 23–30 (1966).
48. Ozawa, M., & Morimoto, H. Effects of various fibres on high-temperature spalling in high-performance concrete. *Constr. Build. Mater.* **71**, 83–92 (2014).
49. Sertmehmetoglu, Y. On a Mechanism of Spalling of Concrete Under Fire Conditions. (King's College London, 1977).
50. Bažant, Z. P. Analysis of Pore Pressure, Thermal Stress and Fracture in Rapid Heated Concrete. In: *International Workshop on Fire Performance of High-Strength Concrete* (eds. Phan, L. T., Carino, N. J., Duthinh, D. & Garboczi, E.), 155–164 (1998).
51. Lo Monte, F., Felicetti, R., & Miah, M. J. The influence of pore pressure on fracture behaviour of Normal-Strength and High-Performance Concretes at high temperature. *Cem. Concr. Compos.* **104**, (2019).
52. Choe, G. *et al.* Effect of moisture migration and water vapor pressure build-up with the heating rate on concrete spalling type. *Cem. Concr. Res.* **116**, 1–10 (2019).
53. Justs, J., Wyrzykowski, M., Bajare, D., & Lura, P. Internal curing by superabsorbent polymers in ultra-high performance concrete. *Cem. Concr. Res.* **76**, 82–90 (2015).
54. Dauti, D. *et al.* Modeling concrete exposed to high temperature : Impact of dehydration and retention curves on moisture migration. *Int. J. Numer. Anal. Methods Geomech.* **42**, 1516–1530 (2018).
55. Diamond, S. Mercury porosimetry. An inappropriate method for the measurement of pore size distributions in cement-based materials. *Cement and Concrete Research,* **30**, 1517–1525 (2000).
56. Kaufmann, J., Loser, R., & Leemann, A. Analysis of cement-bonded materials by multi-cycle mercury intrusion and nitrogen sorption. *J. Colloid Interface Sci.* **336**, 730–7 (2009).
57. Washburn, E. Note on a Method of Determining the Distribution of Pore Sizes in a Porous Material. *Proc Natl Acad Sci* **7**, 115–116 (1921).

58. Winslow, D. N., & Diamond, S. A mercury porosimetry study of the porosity in Portland cement. *J. Mater.* 564–585 (1970).
59. Hearn, N., & Hooton, R. D. Sample mass and dimension effects on mercury intrusion porosimetry results. *Cem. Concr. Res.* **22**, 970–980 (1992).
60. Kaufmann, J. Pore space analysis of cement-based materials by combined Nitrogen sorption – Wood's metal impregnation and multi-cycle mercury intrusion. *Cem. Concr. Compos.* **32**, 514–522 (2010).
61. Kaufmann, J. Characterization of Pore Space of Cement-Based Materials by Combined Mercury and Wood's Metal Intrusion. *J. Am. Ceram. Soc.* **92**, 209–216 (2009).
62. Lehmann, E., Vontobel, P., & Wiezel, L. Properties of the radiography facility NEUTRA at SINQ and its potential for use as European reference facility. *Nondestruct. Test.* 191–202 (2001).
63. Weber, B. *et al.* Neutron radiography of heated high-performance mortar. *MATEC Web Conf.* **6**, 03004 (2013).
64. Toropovs, N. *et al.* Real-time measurements of temperature, pressure and moisture profiles in High-Performance Concrete exposed to high temperatures during neutron radiography imaging. *Cem. Concr. Res.* **68**, 166–173 (2015).
65. Dauti, D. *et al.* Analysis of moisture migration in concrete at high temperature through in-situ neutron tomography. *Cem. Concr. Res.* (2018). doi:10.1016/J.CEMCONRES.2018.06.010
66. Dauti, D. *et al.* First results on fast neutron tomography of heated concrete. in *5th International Workshop on Concrete Spalling due to Fire Exposure,* 249–258 (2017).
67. Dauti, D., Dal Pont, S., Briffaut, M., & Weber, B. Modeling of 3D moisture distribution in heated concrete: From continuum towards mesoscopic approach. *Int. J. Heat Mass Transf.* **134**, 1137–1152 (2019).
68. Dauti, D. *et al.* Some Observations on Testing Conditions of High-Temperature Experiments on Concrete: An Insight from Neutron Tomography. *Transp. Porous Media,* **132**, 299–310 (2020).
69. Lura, P., & Terrasi, G. Pietro. Reduction of fire spalling in high-performance concrete by means of superabsorbent polymers and polypropylene fibers: Small scale fire tests of carbon fiber reinforced plastic-prestressed self-compacting concrete. *Cem. Concr. Compos.* **49**, 36–42 (2014).
70. Sedighi-Gilani, M. *et al.* Visualization and quantification of liquid water transport in softwood by means of neutron radiography. *Int. J. Heat Mass Transf.* **55**, 6211–6221 (2012).
71. Lukić, B., Tengattini, A., Dufour, F., & Briffaut, M. Visualising water vapour condensation in cracked concrete with dynamic neutron radiography. *Mater. Lett.* **283**, 1–4 (2021).
72. Kalifa, P., Chéné, G., & Gallé, C. High-temperature behavior of HPC with polypropylene fibers from spalling to microstructure. *Cem. Concr. Res.* **31**, 1487–1499 (2001).
73. Pimienta, L. *et al.* Evolution in Seismic Properties During Low and Intermediate Water Saturation: Competing Mechanisms During Water Imbibition? *Geophys. Res. Lett.* **46**, 4581–4590 (2019).
74. Payan, C., Ulrich, T. J., Le Bas, P. Y., Saleh, T., & Guimaraes, M. Quantitative linear and nonlinear resonance inspection techniques and analysis for material characterization:

Application to concrete thermal damage. *J. Acoust. Soc. Am.* **136**, 537–546 (2014).
75. Haupert, S. *et al.* High-accuracy acoustic detection of nonclassical component of material nonlinearity. *J. Acoust. Soc. Am.* **130**, 2654–61 (2011).
76. Khatib, J. M., Herki, B. A., & Elkordi, A. *Characteristics of concrete containing EPS*. *Use of Recycled Plastics in Eco-efficient Concrete* (Elsevier Ltd, 2019). doi:10.1016/b978-0-08-102676-2.00007-4
77. Ma, G. *et al.* Physical, mineralogical, thermal, and mechanical properties of aerogel-incorporated concrete exposed to elevated temperatures. *Cem. Concr. Compos.* **140**, 105089 (2023).
78. Jensen, O. M., & Hansen, P. F. Water-entrained cement-based materials: II. Experimental observations. *Cem. Concr. Res.* **32**, 973–978 (2002).
79. Zhong, P. *et al.* Internal curing with superabsorbent polymers of different chemical structures. *Cem. Concr. Res.* **123**, (2019).
80. Boshoff, W. *et al.* The effect of superabsorbent polymers on the mitigation of plastic shrinkage cracking of conventional concrete, results of an inter-laboratory test by RILEM TC 260-RSC. *Mater. Struct. Constr.* **53**, (2020).
81. Bernard, E., Jenni, A., Toropovs, N., & Mäder, U. Percolation experiment across a 10-year-old interface between Opalinus Clay and Portland concrete. *Cem. Concr. Res.* **170**, (2023).

Nikolajs Toropovs was born in 1986 in Riga. He received a Bachelor's degree in Construction Science (2007) and a Master's degree in Civil Engineering (2012) from Riga Technical University. During his studies, he worked at the Faculty of Civil Engineering of RTU. Since 2016, he has been a researcher at the Swiss Federal Laboratories for Materials Science and Technology. In 2025, he received the Swiss Building Award.